https://dx.doi.org/10.1016/j.compositesb.2019.01.072

Nonlinear dynamic behavior of single-layer graphene under uniformly distributed loads

J.W. Yan[1,2], S.K. Lai[3,4,*], L.H. He[2,5]

[1] Key Laboratory of Product Packaging and Logistics of Guangdong Higher Education Institutes, Jinan University, Zhuhai, Guangdong, P.R. China

[2] MOE Key Lab of Disaster Forecast and Control in Engineering, Jinan University, Guangzhou, Guangdong, P.R. China

[3] Department of Civil and Environmental Engineering, The Hong Kong Polytechnic University, Hung Hom, Kowloon, Hong Kong, P.R. China

[4] The Hong Kong Polytechnic University Shenzhen Research Institute, Nanshan, Shenzhen, P.R. China

[5] CAS Key Laboratory of Mechanical Behavior and Design of Materials, Department of Modern Mechanics, University of Science and Technology of China, Anhui, P.R. China

Abstract

An atomistic-continuum multiscale approach is developed to simulate the nonlinear dynamic behavior of simply-supported single layer graphene sheets subject to a uniformly distributed out-of-plane load. The dynamic equation of motion is derived and solved by the Newmark-β method. The evolution of surface morphology and the nonlinear effect in terms of geometric and material nonlinearities can be captured by iteratively updating the system stiffness. It is found that the natural frequency of simply-supported graphene sheets almost remains constant when the external load is in a small range. The present solutions are in good agreement with those results obtained from the

*Corresponding author. E-mail: sk.lai@polyu.edu.hk (S.K. Lai)

linear vibration analysis by a semi-analytical method. As the applied load increases continuously, this gives rise to an elongation of graphene to increase the natural frequency. Based on the numerical approach, the surface morphology evolution of graphene can be visualized and explored.

Keywords: Graphene; Nonlinear dynamic behavior; Atomistic-continuum multiscale approach; Natural frequency; Surface morphology evolution

1. Introduction

Graphene exfoliated from bulk graphite is the first isolated two-dimensional material with a hexagonal lattice [1, 2]. Since the discovery of graphene, its superior properties in chemical, electrical and mechanical aspects have advanced various fields in nanoscience and nanotechnology. Many scholars have devoted great efforts on graphene and countless research findings have unfolded the significance of this new carbon allotrope. Among various promising applications of graphene, one important usage is in nano-electromechanical systems (NEMS) [3-8], involving electromagnetic sensors [3], advanced resonators [5], energy harvesters [7] and bistable actuator [8]. This is mainly due to its high Young's modulus (in TPa order) and ultrahigh resonance frequency (in THz order). In addition, graphene is also an ideal hydrogen storage material as it has a large surface area to absorb hydrogen atoms [9, 10]. Hence, a comprehensive study for the dynamic characteristics of graphene, especially the large amplitude vibration behaviors [11-15], is highly desired for the design of nano-devices.

A series of theoretical studies have been reported on the vibration behavior of graphene such as *ab* initio methods, density functional theory simulations, molecular mechanics/dynamics, space frame approach, and classical/nonlocal continuum models. He et al. [16] used a stacked plate model to investigate the linear vibration of multi-layer graphene sheets. They found that the van der Waals interaction does not have influence on the lowest natural frequency, but it can significantly affect the higher-order natural frequencies. Subsequently, they also studied the nonlinear forced vibration of multi-layer graphene sheets [17], in which the research finding can be applied to design

the separation of a multi-layer graphene sheet into a few-layer or even a single-layer. Mianroodi et al. [18] adopted a membrane model to study the large amplitude vibration of single layer graphene sheets. By increasing either the pre-tension or the initial velocity can enhance the nonlinear fundamental frequency of graphene sheets, the former one plays a dominant role and can weaken the effect of the latter one to a negligible effect.

In addition, Sadeghi and Naghdabadi [19] introduced a hybrid atomistic-structural element that is capable of modelling nonlinear behavior of graphene sheets. Singh and Patel [20] employed a multi-scale model to incorporate the Cauchy-Born rule with a standard finite element method for the nonlinear analysis of graphene sheets. The results showed that the geometric nonlinearity contributes a dominant hardening effect as compared to the material nonlinearity. It is also found that the graphene sheets with simply-supported constraints can also exhibit a greater hardening nonlinear effect than those with clamped boundaries. Along with the nonlocal elasticity theory, Shen et al. [21] used molecular dynamics simulations to study the nonlinear transverse vibration response of bilayer graphene sheets in thermal environments. They pointed out that the nonlinear vibration response of bilayer graphene sheets is much sensitive to the small scale effect as well as the temperature change, but it is not dependent on the nonlinear van der Waals interaction coefficient. Furthermore, Naderi and Saidi [22] studied the nonlocal postbuckling behavior of both uniaxially and biaxially loaded graphene sheets in a nonlinear polymer medium. Zhu et al. [10] also investigated the nonlinear dynamics and bifurcation of Al-doped graphene impacted by hydrogen atoms.

The aforementioned studies emphasized on the significance of the nonlinear vibration characteristics of graphene in many engineering applications. Among all methods employed, atomistic-based methods are successful to trace atomic trajectories but at the cost of high computational resource. In addition, continuum methods always work with the help of introducing some external parameters, which are not stationary and size-dependent, e.g., elastic constants. In this paper, we use a bottom-up method, namely the atomistic-continuum multiscale method [23, 24], for the nonlinear vibration analysis of simply-supported graphene sheets. This newly developed approach not only takes the advantage of tracing atomic trajectories as an atomistic-based method, and also it possesses high-performance computation as a continuum method.

The atomistic-continuum multiscale method incorporates the higher-order Cauchy-Born rule to link the deformation of covalent bond vectors and the macroscopical deformation gradients. On one hand, the real nonlinear stress-strain relationship is directly obtained from the atomic interactions, which can be described by the widely used Tersoff-Brenner empirical interatomic potential [25, 26]. Therefore, the material nonlinearity can be captured by updating the built stiffness matrix at each iterative time step. On the other hand, the built stiffness matrix that depends on the involved higher-order gradients has a significant effect when studying the large amplitude vibration of graphene sheets. The Newmark-β method [27] is then used to solve the dynamic equation, and thus the real-time morphology evolution of simply-supported single layer graphene sheets under arbitrary external excitations can be traced. Moreover, the effects of both geometric and material nonlinearities are captured to

investigate its dynamic properties. By using the fast Fourier transform algorithm, the forcing natural frequencies of graphene sheets can also be determined.

2. Atomistic-continuum approach

2.1 Higher-order Cauchy-Born rule

A two-dimensional initial equilibrium planar graphene can be described by introducing three geometrical parameters λ_1, λ_2, and θ, which are the uniform longitudinal stretch, transverse stretch and shear strain, respectively. According to the repeated hexagonal lattice of a graphene sheet, i.e., the branch-like structure in Fig. 1, the center atom covalently surrounded by three neighboring atoms with an angle of 120° is selected as a representative cell. The mapping relationship between the initial equilibrium graphene and the reference one is [24]

$$\begin{cases} x_1 = \lambda_1 X_1 \\ x_2 = \lambda_1 X_1 \sin\theta + \lambda_2 X_2 \end{cases} \tag{1}$$

in which $\mathbf{x} = \mathbf{x}\left(x_1, x_2\right)$ and $\mathbf{X} = \mathbf{X}\left(X_1, X_2\right)$ are nodal coordinates in the initial equilibrium and reference configurations, respectively.

A recently developed multiscale method, namely the atomistic-continuum multiscale approach [24], is on the basis of the Cauchy-Born rule. Such a rule can offer a refined linkage between the deformation of lattice vectors at a nanoscale and the deformation gradients in a macroscopic continuum field. When this Cauchy-Born rule is directly used to study one-atomic thick structures, e.g., carbon nanotube and graphene, a zero bending stiffness is found [28]. To overcome this challenge, the higher-order gradient Cauchy-Born rule was proposed to capture the bending effect [29, 30]. Based

on the modified Cauchy-Born rule, Sun and Liew [31, 32] developed a mesh-free computational framework to realize the whole numerical simulation for buckling analysis of carbon nanotubes. This multiscale approach can exhibit superior computational performance as the numerical simulation is carried out at a macroscopic continuum viewpoint rather than at a nanoscale. Moreover, it can capture the information of atomic structures and its atomic interactions.

Owing to the Bravais multi-lattice characteristics in graphene, it is non-centrosymmetric in nature. In order to maintain the minimum potential of a system, an inner shift vector $\boldsymbol{\eta}$ is introduced. The bond vector between I^{th} and J^{th} atoms in the current configuration $\mathbf{r}_{IJ}$ can be calculated by that in the reference one $\mathbf{R}_{IJ}$ as [33]

$$\mathbf{r}_{IJ} = \mathbf{F}\cdot(\mathbf{R}_{IJ}+\boldsymbol{\eta}) + \frac{1}{2}\mathbf{G}:[(\mathbf{R}_{IJ}+\boldsymbol{\eta})\otimes(\mathbf{R}_{IJ}+\boldsymbol{\eta})] \tag{2}$$

in which $\mathbf{F} = \dfrac{\partial \mathbf{x}}{\partial \mathbf{X}}$ and $\mathbf{G} = \dfrac{\partial^2 \mathbf{x}}{\partial \mathbf{X}^2}$ are, respectively, the first-order and second-order deformation gradient tensors determined by the macroscopic continuum deformation in Eq. (1).

As a widely used empirical potential, the Tersoff-Brenner multi-body potential is applied to calculate the atomic interactions [25, 26], and the second set of parameters is employed in this study. The energy stored in the system is a function of the bond energy and the energy per atom, it can be calculated by adding the neighboring three bond energy levels together as follows

$$W_{\mathrm{I}}(\mathbf{F},\mathbf{G},\boldsymbol{\eta}) = \frac{1}{2}\sum_{\mathrm{J}=1}^{3} V_{\mathrm{IJ}}(\mathbf{r}_{\mathrm{I2}},\mathbf{r}_{\mathrm{I2}},\mathbf{r}_{\mathrm{I3}}) = V_{\mathrm{I}}[\mathbf{F},\mathbf{G},\boldsymbol{\eta}] \tag{3}$$

As indicated, the hexagonal lattice of graphene is not centrosymmetric. For a given

deformation description, the inner shift $\boldsymbol{\eta}$ can be determined by

$$\frac{\partial V_{\mathrm{I}}}{\partial \boldsymbol{\eta}} = \mathbf{0} \tag{4}$$

Equations (3) and (4) imply that the strain energy is only dependent on the first-order and second-order deformation gradients **F** and **G**.

Define the area strain energy density as

$$\omega_{\mathrm{I}}(\mathbf{F},\mathbf{G}) = \frac{W_{\mathrm{I}}[\mathbf{F},\mathbf{G},\boldsymbol{\eta}(\mathbf{F},\mathbf{G})]}{\Omega_1}, \quad v_{\mathrm{I}} = \frac{V_{\mathrm{I}}[\mathbf{F},\mathbf{G},\boldsymbol{\eta}(\mathbf{F},\mathbf{G})]}{\Omega_1} \tag{5}$$

in which Ω_1 is the average area per atom $\frac{3\sqrt{3}}{4} r_0^2$ with r_0 being the C-C bond length in the initial configuration. To obtain the initial equilibrium configuration of graphene, we minimize the potential of those representative cells. An arbitrary initial guess of the C-C bond length can be used without any influence on the initial equilibrium configuration. In the present study, the C-C bond length is semi-analytically determined to be 0.14507 nm.

For the sake of completeness, the vector $\mathbf{grad} = [\mathbf{F}\ \ \mathbf{G}]$ denotes a combination of the first-order and second-order deformation gradients. According to Eq. (4), the stress tensor $\boldsymbol{\sigma}$ and the tangential moduli matrix $\mathbf{M}$ can be finally determined [34, 35]

$$\boldsymbol{\sigma} = \frac{\partial \omega_{\mathrm{I}}}{\partial \mathbf{grad}} = \frac{\partial v_{\mathrm{I}}(\mathbf{F},\mathbf{G},\boldsymbol{\eta}(\mathbf{F},\mathbf{G}))}{\partial \mathbf{grad}} = \frac{\partial v_{\mathrm{I}}}{\partial \mathbf{grad}} + \frac{\partial v_{\mathrm{I}}}{\partial \boldsymbol{\eta}} \frac{\partial \boldsymbol{\eta}}{\partial \mathbf{grad}} = \frac{\partial v_{\mathrm{I}}}{\partial \mathbf{grad}} \tag{6}$$

$$\mathbf{M} = \frac{\partial^2 \omega_{\mathrm{I}}}{\partial \mathbf{grad} \otimes \partial \mathbf{grad}} = \frac{\partial}{\partial \mathbf{grad}} \left(\frac{\partial \omega_{\mathrm{I}}}{\partial \mathbf{grad}} \right) = \frac{\partial^2 v_{\mathrm{I}}}{\partial \mathbf{grad} \otimes \partial \mathbf{grad}} + \frac{\partial^2 v_{\mathrm{I}}}{\partial \mathbf{grad} \otimes \partial \boldsymbol{\eta}} \frac{\partial \boldsymbol{\eta}_{\mathrm{I}}}{\partial \mathbf{grad}} \tag{7}$$

From the mapping relationship in Eq. (1), the first-order and second-order deformation gradients are only related to λ_1, λ_2 and θ. Hence, Eq. (5) can be written as

$$v_{\mathrm{I}}[\mathbf{F},\mathbf{G},\boldsymbol{\eta}] = v_{\mathrm{I}}(\lambda_1,\lambda_2,\theta,\eta_1,\eta_2) \tag{8}$$

Denote $\boldsymbol{\lambda}=\boldsymbol{\lambda}\left(\lambda_1,\lambda_2,\theta,\eta_1,\eta_2\right)$, then the geometrical parameters (λ_1, λ_2, θ) and the inner shift variables (η_1,η_2) can be determined by minimizing the potential of a representative cell

$$\frac{\partial v_1}{\partial \boldsymbol{\lambda}}=\mathbf{0} \tag{9}$$

Then, the Newton-Raphson method is applied to iteratively solve Eq. (9).

2.2. Dynamic equation by mesh-free method

The above-mentioned initial equilibrium graphene is used as a reference configuration when studying the surface morphology evolution of graphene sheets under external field stimuli. Consider the deformation process as

$$\begin{cases}\tilde{x}_1=x_1+u_1\\ \tilde{x}_2=x_2+u_2\\ \tilde{x}_3=u_3\end{cases} \tag{10}$$

in which (u_1, u_2, u_3) are the nodal displacements of a relative to its undeformed counterparts along x_1, x_2 and x_3 directions, respectively. The mesh-free method on the basis of a moving Kriging (MK) interpolation [36-38] is adopted to accomplish the nodal displacements

$$\hat{\mathbf{u}}=\hat{\mathbf{u}}(\hat{u}_1,\hat{u}_2,\hat{u}_3)^{\mathrm{T}}=\sum_{\mathrm{i}=1}^{n}\boldsymbol{\phi}_{\mathrm{i}}\mathbf{u}_{\mathrm{i}}=\boldsymbol{\Phi}\mathbf{U} \tag{11}$$

where $\mathbf{u}_{\mathrm{i}}=(u_{\mathrm{i}1},u_{\mathrm{i}2},u_{\mathrm{i}3})^{\mathrm{T}}$ is the i^{th} nodal displacement, while $\boldsymbol{\phi}_{\mathrm{i}}$ is the MK interpolation at the i^{th} node, and n is the total number of nodes covered in the compact support domain. In the MK interpolation, a circular compact support domain is used. The detailed procedures for the MK interpolation can be referred to the previous works, which have been well constructed to model carbon nanotubes and graphene [24, 36,

37].

Based on the Hamilton's principle, the dynamic equation of graphene can be derived. The real solution of the motion during a time period $t_1 \sim t_2$ is determined by the minimization of the Lagrangian function as given by

$$\delta\int_{t_1}^{t_2}(E(t)-W(t)+L(t))\mathrm{d}t=0 \tag{12}$$

where $E(t)$ and $W(t)$ denote the kinetic energy and the elastic energy stored in the system, respectively, while $L(t)$ is the total work done by external forces on the body. The kinetic energy and the elastic energy of the system are given by

$$\delta\int_{t_1}^{t_2}E(t)\mathrm{d}t=\delta\int_{t_1}^{t_2}\int_V\frac{1}{2}\rho\mathbf{U}'(t)^{\mathrm{T}}\mathbf{U}'(t)\mathrm{d}V\mathrm{d}t=-\int_{t_1}^{t_2}\delta(\hat{\mathbf{U}}(t)^{\mathrm{T}})\int_V\rho\boldsymbol{\Phi}^T\boldsymbol{\Phi}\hat{\mathbf{U}}''(t)\mathrm{d}V\mathrm{d}t \tag{13}$$

$$\delta\int_{t_1}^{t_2}W(t)\mathrm{d}t=\delta\int_{t_1}^{t_2}\int_V\frac{1}{2}\mathbf{grad}^{\mathrm{T}}\frac{\partial^2\omega_0}{\partial\mathbf{grad}\partial\mathbf{grad}}\mathbf{grad}\mathrm{d}V\mathrm{d}t=\int_{t_1}^{t_2}\delta(\hat{\mathbf{U}}(t)^{\mathrm{T}})\int_V(\mathbf{L}\boldsymbol{\Phi})^{\mathrm{T}}\mathbf{ML}\boldsymbol{\Phi}\hat{\mathbf{U}}(t)\mathrm{d}V\mathrm{d}t \tag{14}$$

$$\delta\int_{t_1}^{t_2}L(t)\mathrm{d}t=\delta\int_{t_1}^{t_2}\int_V\mathbf{U}(t)^{\mathrm{T}}\mathbf{f}(t)\mathrm{d}V\mathrm{d}t=\int_{t_1}^{t_2}\delta(\hat{\mathbf{U}}(t)^{\mathrm{T}})\int_V\boldsymbol{\Phi}^{\mathrm{T}}\mathbf{f}(t)\mathrm{d}V\mathrm{d}t \tag{15}$$

where ρ is the area mass density calculated by m_{c}/Ω_1 with m_{c} being 1.9943×10^{-23} g.

Substituting Eqs. (13)-(15) into Eq. (12), we have

$$\int_{t_1}^{t_2}\delta(\hat{\mathbf{U}}(t)^{\mathrm{T}})\int_V\rho\boldsymbol{\Phi}^{\mathrm{T}}\boldsymbol{\Phi}\hat{\mathbf{U}}''(t)\mathrm{d}V\mathrm{d}t+\int_{t_1}^{t_2}\delta(\hat{\mathbf{U}}(t)^{\mathrm{T}})\int_V(\mathbf{L}\boldsymbol{\Phi})^{\mathrm{T}}\mathbf{ML}\boldsymbol{\Phi}\hat{\mathbf{U}}(t)\mathrm{d}V\mathrm{d}t=\int_{t_1}^{t_2}\delta(\hat{\mathbf{U}}(t)^{\mathrm{T}})\int_V\boldsymbol{\Phi}^{\mathrm{T}}\mathbf{f}(t)\mathrm{d}V\mathrm{d}t \tag{16}$$

Thus, the dynamic equation of the system becomes

$$\int_V[\rho\boldsymbol{\Phi}^{\mathrm{T}}\boldsymbol{\Phi}\hat{\mathbf{U}}''(t)+(\mathbf{L}\boldsymbol{\Phi})^{\mathrm{T}}\mathbf{ML}\boldsymbol{\Phi}\hat{\mathbf{U}}(t)]\mathrm{d}V=\int_V\boldsymbol{\Phi}^{\mathrm{T}}\mathbf{f}(t)\mathrm{d}V \tag{17}$$

The Newmark-β method [27] is then employed to solve Eq. (17). We assume that a linear variation of the accelerated velocity during the time period $t \sim t+\Delta t$ is

$$\hat{\mathbf{U}}'(\mathrm{t}+\Delta\mathrm{t})=\hat{\mathbf{U}}'(\mathrm{t})+\left[(1-\delta)\hat{\mathbf{U}}''(\mathrm{t})+\delta\hat{\mathbf{U}}''(\mathrm{t}+\Delta\mathrm{t})\right]\Delta\mathrm{t} \tag{18}$$

$$\hat{\mathbf{U}}(\mathrm{t}+\Delta\mathrm{t})=\hat{\mathbf{U}}(\mathrm{t})+\hat{\mathbf{U}}'(\mathrm{t})\Delta\mathrm{t}+\left[\left(\frac{1}{2}-\beta\right)\hat{\mathbf{U}}''(\mathrm{t})+\beta\hat{\mathbf{U}}'(\mathrm{t}+\Delta\mathrm{t})\right]\Delta\mathrm{t}^2 \tag{19}$$

Then, the accelerated velocity and the velocity can be expressed as,

$$\hat{\mathbf{U}}''(\mathrm{t}+\Delta\mathrm{t})=\frac{1}{\beta\Delta\mathrm{t}^2}\left(\hat{\mathbf{U}}(\mathrm{t}+\Delta\mathrm{t})-\hat{\mathbf{U}}(\mathrm{t})\right)-\frac{1}{\beta\Delta\mathrm{t}}\hat{\mathbf{U}}'(\mathrm{t})-\left(\frac{1}{2\beta}-1\right)\hat{\mathbf{U}}''(\mathrm{t}) \tag{20}$$

$$\hat{\mathbf{U}}'(\mathrm{t}+\Delta\mathrm{t})=\frac{1}{\beta\Delta\mathrm{t}}\left(\hat{\mathbf{U}}''(\mathrm{t}+\Delta\mathrm{t})-x_{\mathrm{t}}\right)+\left(1-\frac{\delta}{\beta}\right)\hat{\mathbf{U}}'(\mathrm{t})+\left(1-\frac{1}{2\beta}\right)\Delta\mathrm{t}\hat{\mathbf{U}}''(\mathrm{t}) \tag{21}$$

Based on Eqs. (20) and (21), the dynamic equation (17) at the time step $t+\triangle t$ can then be re-written as

$$\hat{\mathbf{K}}(\mathrm{t}+\Delta\mathrm{t})\cdot\hat{\mathbf{U}}(\mathrm{t}+\Delta\mathrm{t})=\hat{\mathbf{f}}(\mathrm{t}+\Delta\mathrm{t}) \tag{22}$$

in which

$$\hat{\mathbf{K}}(\mathrm{t}+\Delta\mathrm{t})=\int_{\mathrm{V}}[(\mathbf{L}\boldsymbol{\Phi})^{\mathrm{T}}\mathbf{M}(\mathrm{t}+\Delta\mathrm{t})\mathbf{L}\boldsymbol{\Phi}]\mathrm{dV}+\frac{\delta}{\beta\Delta\mathrm{t}^2}\int_{\mathrm{V}}[\rho\boldsymbol{\Phi}^{\mathrm{T}}\boldsymbol{\Phi}]\mathrm{dV} \tag{23}$$

$$\hat{\mathbf{f}}(\mathrm{t}+\Delta\mathrm{t})=\int_{\mathrm{V}}\boldsymbol{\Phi}^{\mathrm{T}}\mathbf{f}(\mathrm{t}+\Delta\mathrm{t})\mathrm{dV}+\int_{\mathrm{V}}[\rho\boldsymbol{\Phi}^{\mathrm{T}}\boldsymbol{\Phi}]\mathrm{dV}\left[\frac{1}{\beta\Delta\mathrm{t}^2}\hat{\mathbf{U}}(\mathrm{t})+\frac{1}{\beta\Delta\mathrm{t}}\hat{\mathbf{U}}'(\mathrm{t})+\left(\frac{1}{2\beta}-1\right)\hat{\mathbf{U}}''(\mathrm{t})\right] \tag{24}$$

Assume $\mathbf{f}(t)=0$, Eq. (17) is then degenerated to a linear free vibration problem. Consider the field function $\hat{\mathbf{U}}(t)=\mathbf{A}exp(i\omega t)$, Eq. (17) can be re-written as:

$$\int_{V}[(\mathbf{L}\boldsymbol{\Phi})^{\mathrm{T}}\mathbf{M}\mathbf{L}\boldsymbol{\Phi}-\omega^2\rho\boldsymbol{\Phi}^{\mathrm{T}}\boldsymbol{\Phi}]\hat{\mathbf{U}}\mathrm{d}V=0 \tag{25}$$

where $\omega=2\pi f$ is an angular frequency. For brevity and simplification, we define

$$\mathbf{K}=\int_{V}(\mathbf{L}\boldsymbol{\Phi})^{\mathrm{T}}\mathbf{M}\mathbf{L}\boldsymbol{\Phi}\mathrm{d}V\text{, and }\mathbf{M}_{\mathrm{A}}=\int_{V}\rho\boldsymbol{\Phi}^{\mathrm{T}}\boldsymbol{\Phi}\mathrm{d}V \tag{26}$$

In Eq. (25), the natural frequencies and its associated vibration modes can be obtained by using a semi-analytical method. In the linear vibration analysis, both geometric and material nonlinearities are neglected and the results are used for comparison.

3. Results and Discussion

In this section, numerical simulations based on the above-mentioned approach for the nonlinear free vibration of simply-supported rectangular graphene sheets are carried out. Besides, the linear free vibration analysis is also conducted for comparison. A numerical scheme with $m \times m$ nodes along both longitudinal and transverse directions of a simply-supported graphene sheet is considered.

In many previous studies, it is found that the chirality is an insignificant factor on the mechanical behavior of graphene. Therefore, this paper focuses on the effect of graphene size but not the type of graphene. A graphene type (n, n)/(n, 0) with n hexagons along both armchair and zigzag edges is selected for analysis. Figure 1 shows a schematic diagram for a (10, 10)/(10, 0) graphene sheet. Using the atomistic-continuum approach, the bond length $r_{\text{c-c}}$ in the initial equilibrium graphene is determined to be ~0.14507 nm by a structural optimized process. Hence, the size of a (n, n)/(n, 0) graphene sheet can be evaluated by $3nr_{c-c} \times \sqrt{3}nr_{c-c}$.

The linear free vibration of graphene sheets, in terms of natural frequency and vibration mode, can be performed as described in Section 2. A series of nodal arrangement schemes are conducted for comparison and convergence studies. The first ten natural frequencies for the linear free vibration of simply-supported graphene sheets with different sizes, i.e., (10, 10)/(10, 0) and (20, 20)/(20, 0), are listed in Tables 1 and 2, respectively. Only a slight deviation occurs in the 9×9 case as compared to other cases, the tabulated data are quite closed to confirm its good accuracy and computational stability. It is independent of the system size in the present atomistic-continuum approach. Such an exciting computational accuracy with high performance

examines this atomistic-continuum multiscale approach to be promising for a whole numerical simulation in large and complex systems as compared with the atomistic simulation approaches, e.g., *ab* initio methods and classical molecular dynamics. For example, a (10, 10)/(10, 0) graphene sheet contains 420 atoms and thus the degree of freedom of the system is 420×3 in atomistic simulation, while which is only 169×3 in our present multiscale method when using the 13×13 nodal scheme. When the sample increases to a (20, 20)/(20, 0) graphene sheet, the degree of freedom of the system increases up to 1640×3 in atomistic simulation, while the 13×13 nodal scheme in the multiscale method can steadily achieve a good prediction for the nonlinear dynamic behavior of graphene. Another key issue of the atomistic simulation approaches is the small time step problem, which can often limit the study to a nano-second level problem. It is required to set as 1 *f*s due to the limit of lattice sizes. However, it is beneficial from the larger distance between neighboring nodes in the multiscale method than that of the lattice constants, the time step can be up to 5 *f*s for simulating (10, 10)/(10, 0) graphene, and even continuously increases to 10 *f*s for (20, 20)/(20, 0) graphene without influencing the accuracy of capturing the nonlinear effects (as discussed in Figs. 3 and 8). The first twelve vibration mode shapes of (10, 10)/(10, 0) simply-supported graphene sheets are also plotted in Fig. 2.

The real-time morphology evolution of graphene under external out-of-plane loads, involving geometrical and material nonlinearities, can be iteratively calculated by the Newmark-β method. Fig. 3 shows the deflection at the midpoint of (20, 20)/(20, 0) simply-supported graphene sheets under two different out-of-plane uniformly

distributed loads (10^{-3} eV/nm^3 and 10^{-2} eV/nm^3). The curves almost coalesce together in both figures, this confirms the present atomistic-continuum multiscale approach with good convergence to investigate the dynamic behavior of graphene again. The enlarged drawing in Fig. 3(a) demonstrates that the nodal schemes 9×9 and 11×11 sit nearly on the two sides of the other three schemes, while the nodal scheme 9×9 is parallel to the other four schemes but with no conspicuous deviation in Fig. 3(b). It is also noteworthy that the wavenumber increases during the same simulation time as the external load increases. In other words, the nonlinear effect becomes noticeable as the external load increases, and it plays a significant role on the natural frequency of graphene. In the subsequent analysis, the nodal scheme 13×13 is adopted to investigate the nonlinear effect in terms of geometric and material properties on the dynamic behavior of graphene.

The effect of nonlinearity is closely related to the deformation of graphene subject to external loads. Figure 4 demonstrates the deflection at the midpoint of (20, 20)/(20, 0) simply-supported graphene sheets under various uniformly distributed out-of-plane loads, ranging from 10^{-5} to 10^{-2} eV/nm^3. The time step is set as 10 *f*s. As mentioned before, the wavenumber increases as the external load increases. By using the fast Fourier transform algorithm, the corresponding frequency spectra for simply-supported graphene sheets under various external loads are presented in Figure 5. It is obvious that the highest peak occurs at 0 Hz. This is because that the graphene sheets will seek a new equilibrium state to adapt the imposed loads. In terms of a physical perspective, the motion of the system contains not only periodic vibration but also translation motion

under a constant load, of which the period is infinitely long. In Fig. 5, the curves show that the translation motion pre-dominates most of the system energy and then the fundamental vibration. In another aspect, as shown in Fig. 4, the dynamic deflection at the midpoint of the graphene sheets under a load of 0.01 eV/nm^3 is ~0.059 nm, which corresponds to a static deflection of graphene under a load of 0.02 eV/nm^3 [24], as expected. The curves demonstrate that the fundamental frequency is extracted to be 0.0354 THz when a small load (e.g., 10^{-5} eV/nm^3) is imposed. This is in good agreement with the linear free vibration analysis, i.e., 0.0348 THz with less than a 2% difference. As the external load increases, the fundamental frequency increases slowly first and then sharply when the load is larger than 10^{-2} eV/nm^3. When the load increases to 10^{-2} eV/nm^3, the fundamental frequency increases to 0.0638 THz accordingly, with about an 80% amplification. We also found that the amplitude increases almost linearly when the load is less than 10^{-3} eV/nm^3, see Figs. 5(a)-5(c). This corresponds to a small deformation problem and the elongation of graphene can be neglected with no obvious influence on the results, but the effect becomes nonlinearly when the load goes beyond 10^{-3} eV/nm^3, see Figs. 5(c) and 5(d).

The nonlinear vibration behavior of graphene sheets with different sizes is also investigated in detail. Figures 6-9 depict the time history responses and the corresponding frequency spectra of simply-supported graphene sheets (i.e., (15, 15)/(15, 0) and (10, 10)/(10, 0)) under various uniformly distributed loads. In Figs. 4, 6 and 8, the curves demonstrate that the fluctuation of the deflection at the midpoint of simply-supported graphene sheets becomes pronounced as the external load increases. As a

matter of fact, this is due to the higher-order natural frequencies. When the load increases, the proportion of the second natural frequency becomes larger. From the frequency spectrum curves, it is also found that the decrease of the graphene size gives rise to an increasing effect on the fluctuation. Besides, the same phenomenon that the highest peaks occur at 0 Hz in Fig. 5 is found in both Figs. 7 and 9.

In Figs.10-12, the variation of the fundamental and higher-order natural frequencies of these three types of graphene sheets is presented. These figures clearly show that the fundamental frequencies for these three types of graphene sheets keep almost unchanged when the external load is small. To clearly illustrate this issue, we take the (10, 10)/(10, 0) case as an example. When the external load is 10^{-4} eV/nm^3, the fundamental frequency is 0.1400 THz. It is in good agreement with that obtained from the linear vibration analysis, i.e., 0.1393 THz. When the external load reaches to 10^{-2} eV/nm^3, a hundredfold as large as the previous one, it increases to 0.1440 THz, with only a 3.4% amplification. As the load continues to increase, e.g., 0.05 eV/nm^3, it increases to 0.1821 THz, ~30% amplification, and then to 0.2201 THz as the load increases to 0.1 eV/nm^3, ~58% amplification. The same tendency is also observed in the higher-order natural frequencies for all three sizes of graphene sheets. Besides, they can also be determined by the surface morphology evolution depicted in Fig. 13 as compared with the vibration modes presented in Fig. 2.

In addition, the atomistic-continuum multiscale approach can also be used to trace the evolution of graphene under arbitrary excitations such as pulse excitations. The deflection at the mid-point of these three types of graphene sheets under different pulse

time steps are plotted in Figs. 14-16. Similarly, the fluctuation of the amplitude occurs and becomes evident under the effects of the pulse time and the graphene size. Figures 17-19 show the frequency spectra of simply-supported graphene sheets under different pulse excitations. The relationship between the natural frequency and the pulse time is also illustrated. As expected, the natural frequency increases as the pulse time increases.

4. Concluding remarks

An atomistic-continuum multiscale approach to investigate the nonlinear dynamic behavior of graphene, in terms of both geometric and material nonlinearities, has been developed. The nonlinear effect on the dynamic behavior of graphene can be captured by iteratively updating the system stiffness when it is subject to external loads. As compared with the results obtained by a semi-analytical method, the present method is highly accurate to trace the evolution of surface morphology. The results demonstrate that the nonlinear effect becomes pronounced in both fundamental and higher-order natural frequencies as the external load increases. The size of graphene has also an evident effect on the dynamic behavior. As the graphene size decreases, the proportion of the higher-order natural frequencies becomes larger. The present investigation offers a better understanding for the nonlinear dynamic behavior of graphene sheets.

Acknowledgements

The work described in this paper was fully supported by the research grants from Natural Science Foundation of China (Grant Nos. 11702112 and 11602210) and Natural Science Foundation of Guangdong Province (Nos. 2016A030310090 and 2017A030310183).

References

1. Novoselov, K.S., et al., *Electric Field Effect in Atomically Thin Carbon Films.* Science, 2004. **306**(5696): p. 666-669.
2. Novoselov, K.S., et al., *Two-dimensional atomic crystals.* Proceedings of the National Academy of Sciences of the United States of America, 2005. **102**(30): p. 10451-10453.
3. Reserbat-Plantey, A., et al., *Electromechanical control of nitrogen-vacancy defect emission using graphene NEMS.* Nature Communications, 2016. **7**.
4. Zanjani, M.B., et al., *NEMS With Broken T Symmetry: Graphene Based Unidirectional Acoustic Transmission Lines.* Scientific Reports, 2015. **5**.
5. Bunch, J.S., et al., *Electromechanical resonators from graphene sheets.* Science, 2007. **315**(5811): p. 490-493.
6. Ong, M.T. and E.J. Reed, *Engineered Piezoelectricity in Graphene by Chemical Doping.* Nanotechnology 2012, Vol 1: Advanced Materials, Cnts, Particles, Films and Composites, 2012: p. 161-164.
7. Ong, M.T. and E.J. Reed, *Engineered Piezoelectricity in Graphene.* ACS Nano, 2012. **6**(2): p. 1387-1394.
8. Yi, S.H., X.Q. He, and J. Lu, *Investigation on snapping transitions of locally nanostructured bistable disks actuated by distributed transverse forces.* Mechanics of Materials, 2018. **127**: p. 91-99.
9. Zhu, Z.W., X.M. Li, and J. Xu, *Stochastic nonlinear dynamic characteristics and safe basin of Li-doped graphene impacted by hydrogen atoms.* International Journal of Hydrogen Energy, 2015. **40**(37): p. 12889-12896.
10. Zhu, Z.W., et al., *Nonlinear dynamic characteristics and bifurcation analysis of Al-doped graphene impacted by hydrogen atoms.* International Journal of Hydrogen Energy, 2017. **42**(47): p. 28507-28514.
11. Shen, H.S., X.Q. He, and D.Q. Yang, *Vibration of thermally postbuckled carbon nanotube-reinforced composite beams resting on elastic foundations.* International Journal of Non-Linear Mechanics, 2017. **91**: p. 69-75.
12. Shen, H.S. and X.Q. He, *Large amplitude free vibration of nanotube-reinforced composite doubly curved panels resting on elastic foundations in thermal environments.* Journal of Vibration and Control, 2017. **23**(16): p. 2672-2689.
13. Dong, Y.H., et al., *Nonlinear free vibration of graded graphene reinforced cylindrical shells: Effects of spinning motion and axial load.* Journal of Sound and Vibration, 2018. **437**: p. 79-96.
14. Shen, H.S., et al., *Nonlinear vibration of functionally graded graphene-reinforced composite laminated cylindrical panels resting on elastic foundations in thermal environments.* Composites Part B-Engineering, 2018. **136**: p. 177-186.
15. Zhang, Y., K.M. Liew, and D. Hui, *Characterizing nonlinear vibration behavior of bilayer graphene thin films.* Composites Part B-Engineering, 2018. **145**: p. 197-205.
16. He, X.Q., S. Kitipornchai, and K.M. Liew, *Resonance analysis of multi-layered*

graphene sheets used as nanoscale resonators. Nanotechnology, 2005. **16**(10): p. 2086-2091.
17. He, X.Q., et al., *Analysis of nonlinear forced vibration of multi-layered graphene sheets.* Computational Materials Science, 2012. **61**: p. 194-199.
18. Mianroodi, J.R., et al., *Nonlinear membrane model for large amplitude vibration of single layer graphene sheets.* Nanotechnology, 2011. **22**(30).
19. Sadeghi, M. and R. Naghdabadi, *Nonlinear vibrational analysis of single-layer graphene sheets.* Nanotechnology, 2010. **21**(10): p. 105705.
20. Singh, S. and B.P. Patel, *Nonlinear dynamic response of single layer graphene sheets using multiscale modelling.* European Journal of Mechanics a-Solids, 2016. **59**: p. 165-177.
21. Shen, H.S., Y.M. Xu, and C.L. Zhang, *Prediction of nonlinear vibration of bilayer graphene sheets in thermal environments via molecular dynamics simulations and nonlocal elasticity.* Computer Methods in Applied Mechanics and Engineering, 2013. **267**: p. 458-470.
22. Naderi, A. and A.R. Saidi, *Nonlocal postbuckling analysis of graphene sheets in a nonlinear polymer medium.* International Journal of Engineering Science, 2014. **81**: p. 49-65.
23. Yan, J.W. and K.M. Liew, *Predicting elastic properties of single-walled boron nitride nanotubes and nanocones using an atomistic-continuum approach.* Composite Structures, 2015. **125**: p. 489-498.
24. Yan, J.W., L.W. Zhang, and K.M. Liew, *A multiscale computational framework for the analysis of graphene involving geometrical and material nonlinearities.* Computer Methods in Applied Mechanics and Engineering, 2016. **310**: p. 208-232.
25. Tersoff, J., *New Empirical-Approach for the Structure and Energy of Covalent Systems.* Physical Review B, 1988. **37**(12): p. 6991-7000.
26. Brenner, D.W., *Empirical Potential for Hydrocarbons for Use in Simulating the Chemical Vapor-Deposition of Diamond Films.* Physical Review B, 1990. **42**(15): p. 9458-9471.
27. Newmark, N.M., *A method of computation for structural dynamics*. 1959: American Society of Civil Engineers.
28. Arroyo, M. and T. Belytschko, *Finite element methods for the non-linear mechanics of crystalline sheets and nanotubes.* International Journal for Numerical Methods in Engineering, 2004. **59**(3): p. 419-456.
29. Guo, X., J.B. Wang, and H.W. Zhang, *Mechanical properties of single-walled carbon nanotubes based on higher order Cauchy-Born rule.* International Journal of Solids and Structures, 2006. **43**(5): p. 1276-1290.
30. Wang, J.B., et al., *Energy and mechanical properties of single-walled carbon nanotubes predicted using the higher order Cauchy-Born rule.* Physical Review B, 2006. **73**(11): p. 115428.
31. Sun, Y.Z. and K.M. Liew, *Mesh-free simulation of single-walled carbon nanotubes using higher order Cauchy-Born rule.* Computational Materials Science, 2008. **42**(3): p. 444-452.

32. Sun, Y.Z. and K.M. Liew, *The buckling of single-walled carbon nanotubes upon bending: The higher order gradient continuum and mesh-free method.* Computer Methods in Applied Mechanics and Engineering, 2008. **197**(33-40): p. 3001-3013.
33. Yan, J.W., K.M. Liew, and L.H. He, *Buckling and post-buckling of single-wall carbon nanocones upon bending.* Composite Structures, 2013. **106**: p. 793-798.
34. Liew, K.M. and Y.Z. Sun, *Elastic properties and pressure-induced structural transitions of single-walled carbon nanotubes.* Physical Review B, 2008. **77**(20): p. 205437.
35. Yan, J.W., K.M. Liew, and L.H. He, *Free vibration analysis of single-walled carbon nanotubes using a higher-order gradient theory.* Journal of Sound and Vibration, 2013. **332**: p. 3740-3755.
36. Yan, J.W., K.M. Liew, and L.H. He, *Analysis of single-walled carbon nanotubes using the moving Kriging interpolation.* Computer Methods in Applied Mechanics and Engineering, 2012. **229**: p. 56-67.
37. Yan, J.W., K.M. Liew, and L.H. He, *A mesh-free computational framework for predicting buckling behaviors of single-walled carbon nanocones under axial compression based on the moving Kriging interpolation.* Computer Methods in Applied Mechanics and Engineering, 2012. **247**: p. 103-112.
38. Gu, L., *Moving kriging interpolation and element-free Galerkin method.* International Journal for Numerical Methods in Engineering, 2003. **56**(1): p. 1-11.

Captions of Tables

Table 1 Convergence and comparison of natural frequencies for the linear free vibration of a (10, 10)/(10, 0) simply-supported graphene sheet.

Table 2 Convergence and comparison of natural frequencies for the linear free vibration of a (20, 20)/(20, 0) simply-supported graphene sheet.

Captions of Figures

Fig. 1. Atomic structure of a (10, 10)/(10, 0) graphene sheet.

Fig. 2. Contour plots for the first twelve modes of a (10, 10)/(10, 0) simply-supported graphene sheet.

Fig. 3. Deflection at the midpoint of a (20, 20)/(20, 0) simply-supported graphene sheet subject to (a) 10^{-3} eV/nm^3 and (b) 10^{-2} eV/nm^3. The time step is set as 10 *f*s.

Fig. 4. Time history responses of a (20, 20)/(20, 0) simply-supported graphene sheet under various external loads. The time step is set as 10 *f*s.

Fig. 5. Frequency spectra for a (20, 20)/(20, 0) simply-supported graphene sheet under various external loads.

Fig. 6. Time history responses of a (15, 15)/(15, 0) simply-supported graphene sheet under various external loads. The time step is set as 5 *f*s.

Fig. 7. Frequency spectra for a (15, 15)/(15, 0) simply-supported graphene sheet under various external loads.

Fig. 8. Time history responses of a (10, 10)/(10, 0) simply-supported graphene sheet under various external loads. The time step is set as 5 *f*s.

Fig. 9. Frequency spectra for a (10, 10)/(10, 0) simply-supported graphene sheet under various external loads.

Fig. 10. Linear and nonlinear fundamental frequencies of a (20, 20)/(20, 0) simply-

supported graphene sheet under various external loads.

Fig. 11. Linear and nonlinear fundamental frequencies of a (15, 15)/(15, 0) simply-supported graphene sheet under various external loads.

Fig. 12. Linear and nonlinear fundamental frequencies of a (10, 10)/(10, 0) simply-supported graphene sheet under various external loads.

Fig. 13. Surface morphology evolution of a (10, 10)/(10, 0) simply-supported graphene sheet under a uniformly distributed load of 0.1 eV/nm^3.

Fig. 14. Time history responses of a (20, 20)/(20, 0) simply-supported graphene sheet under 0.01 eV/nm^3 at different pulse time t_h.

Fig. 15. Time history responses of a (15, 15)/(15, 0) simply-supported graphene sheet under 0.1 eV/nm^3 at different pulse time t_h.

Fig. 16. Time history responses of a (10, 10)/(10, 0) simply-supported graphene sheet under 0.1 eV/nm^3 at different pulse time t_h.

Fig. 17. Frequency spectra for a (20, 20)/(20, 0) simply-supported graphene sheet under 0.01 eV/nm^3 at different pulse time (a)-(f), and natural frequency versus pulse time (g).

Fig. 18. Frequency spectra for a (15, 15)/(15, 0) simply-supported graphene sheet under 0.1 eV/nm^3 at different pulse time (a)-(d), and natural frequency versus pulse time (e).

Fig. 19. Frequency spectra for a (10, 10)/(10, 0) simply-supported graphene sheet under 0.1 eV/nm^3 at different pulse time (a)-(d), and natural frequency versus pulse time (e).

Table 1 Convergence and comparison of natural frequencies for the linear free vibration of a (10, 10)/(10, 0) simply-supported graphene sheet.

Mode	Natural frequency (THz)						
No.	9×9	11×11	13×13	15×15	17×17	19×19	25×25
1	0.1379	0.1391	0.1393	0.1393	0.1393	0.1392	0.1390
2	0.2457	0.2459	0.2457	0.2454	0.2451	0.2448	0.2441
3	0.4117	0.4159	0.4172	0.4177	0.4179	0.4179	0.4175
4	0.4444	0.4413	0.4419	0.4435	0.4451	0.4463	0.4484
5	0.5564	0.5572	0.5576	0.5588	0.5594	0.5597	0.5589
6	0.6131	0.6384	0.6473	0.6519	0.6544	0.6558	0.6577
7	0.7259	0.7395	0.7423	0.7436	0.7436	0.7430	0.7396
8	0.8395	0.8974	0.9254	0.9405	0.9460	0.9478	0.9548
9	0.9270	0.9644	0.9515	0.9466	0.9493	0.9544	0.9621
10	0.9929	0.9701	0.9847	0.9897	0.9915	0.9915	0.9879

Table 2 Convergence and comparison of natural frequencies for the linear free vibration of a (20, 20)/(20, 0) simply-supported graphene sheet.

Mode	Natural frequency (THz)						
No.	9×9	11×11	13×13	15×15	17×17	19×19	25×25
1	0.0345	0.0348	0.0348	0.0348	0.0348	0.0348	0.0348
2	0.0614	0.0615	0.0614	0.0614	0.0613	0.0612	0.0610
3	0.1029	0.1040	0.1043	0.1044	0.1045	0.1045	0.1044
4	0.1111	0.1103	0.1105	0.1109	0.1113	0.1116	0.1121
5	0.1391	0.1393	0.1394	0.1397	0.1399	0.1399	0.1397
6	0.1533	0.1596	0.1618	0.1630	0.1636	0.1640	0.1644
7	0.1815	0.1849	0.1856	0.1859	0.1859	0.1858	0.1849
8	0.2099	0.2244	0.2313	0.2351	0.2365	0.2369	0.2387
9	0.2317	0.2411	0.2379	0.2367	0.2373	0.2386	0.2405
10	0.2482	0.2425	0.2462	0.2474	0.2479	0.2479	0.2470

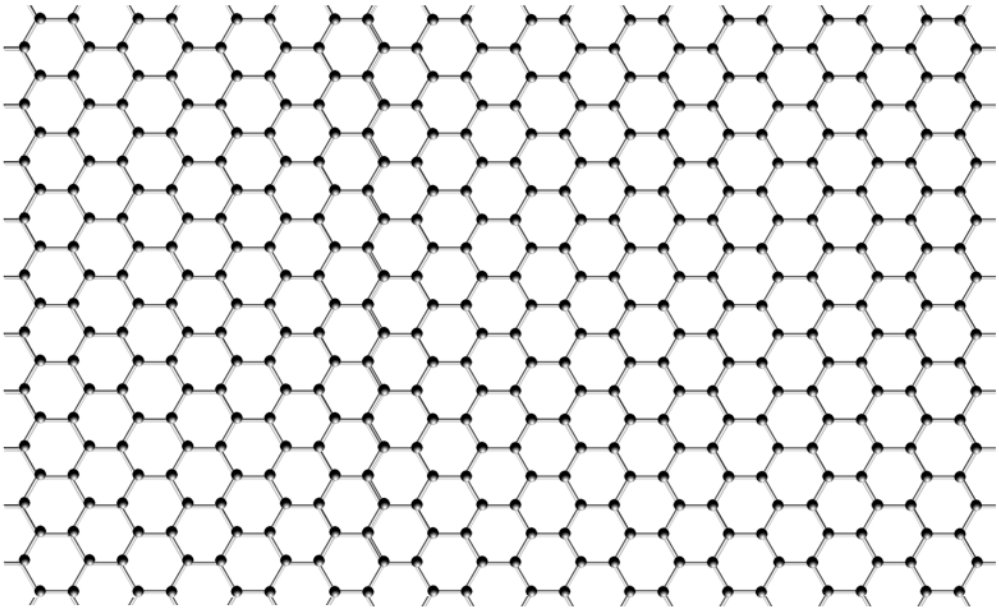

Fig. 1. Atomic structure of a (10, 10)/(10, 0) graphene sheet.

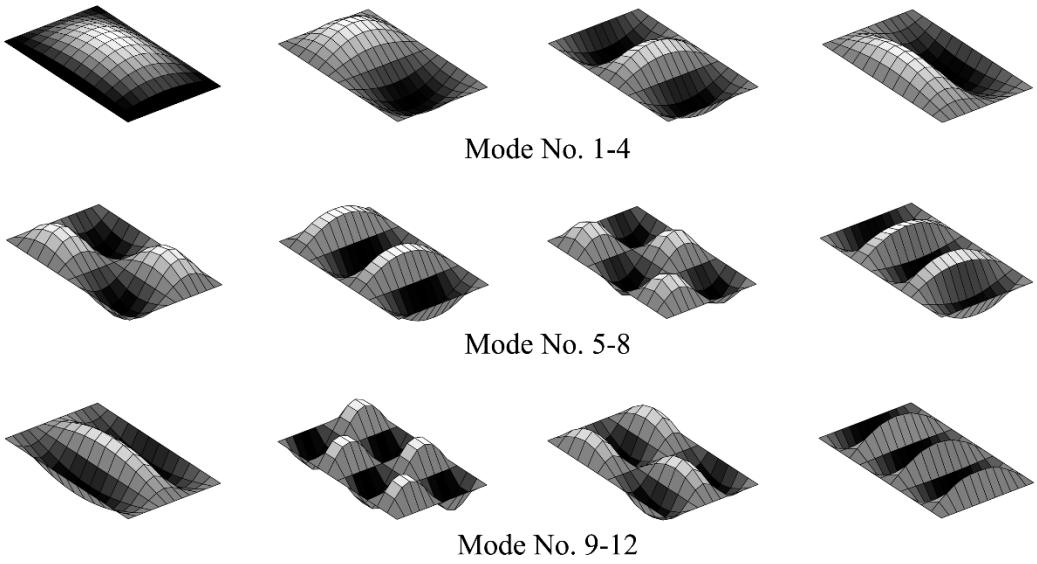

Fig. 2. Contour plots for the first twelve modes of a (10, 10)/(10, 0) simply-supported graphene sheet.

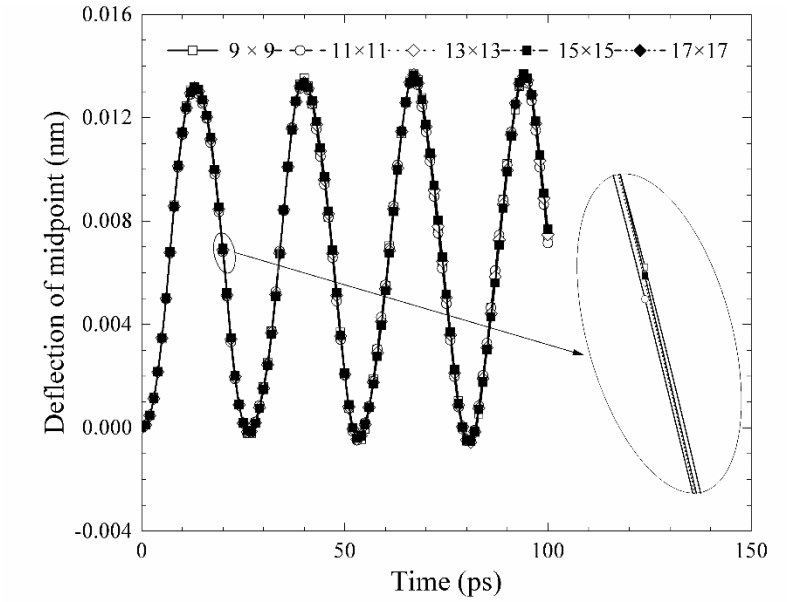

(a)

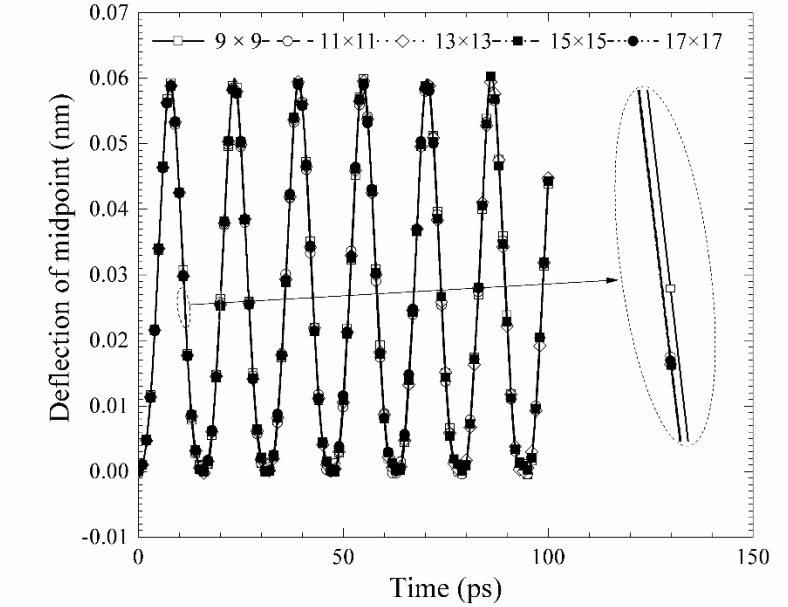

(b)

Fig. 3. Deflection at the midpoint of a (20, 20)/(20, 0) simply-supported graphene sheet subject to (a) 10^{-3} eV/nm^3 and (b) 10^{-2} eV/nm^3. The time step is set as 10 *f*s.

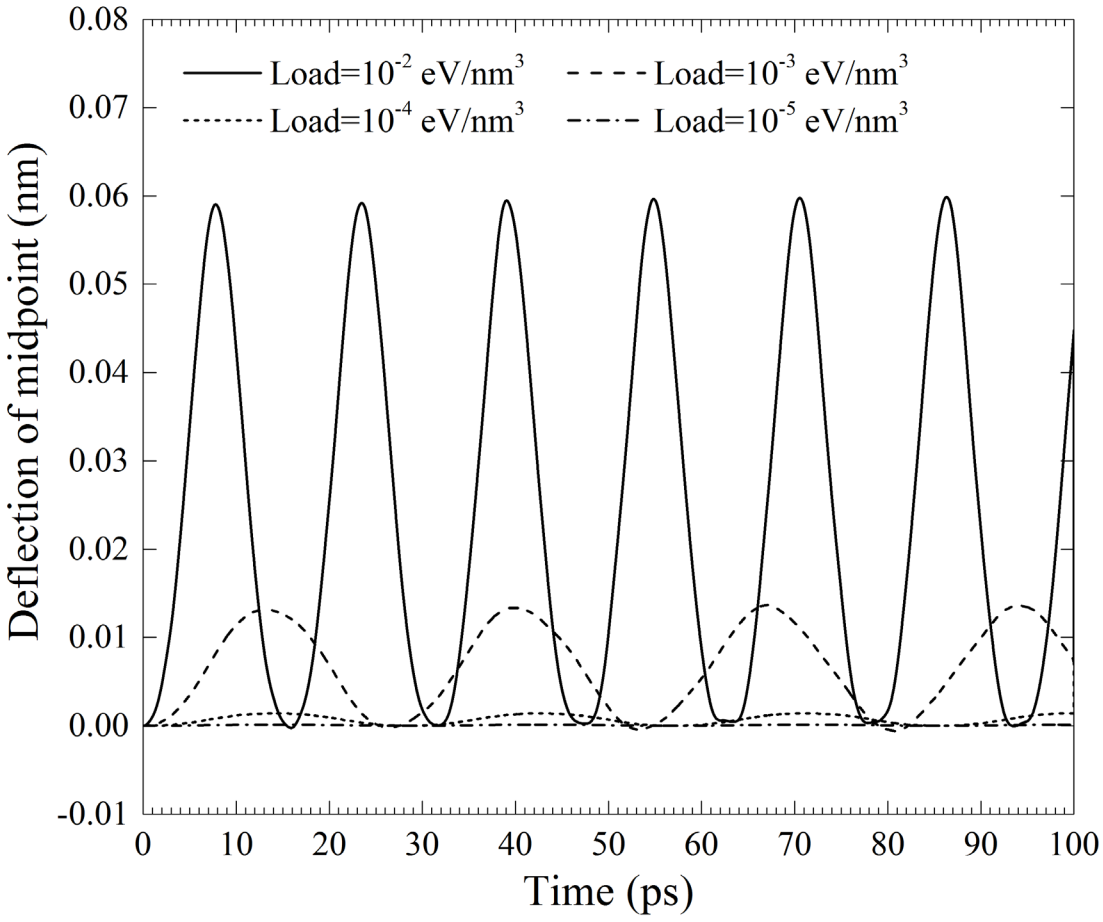

Fig. 4. Time history responses of a (20, 20)/(20, 0) simply-supported graphene sheet under various external loads. The time step is set as 10 *f*s.

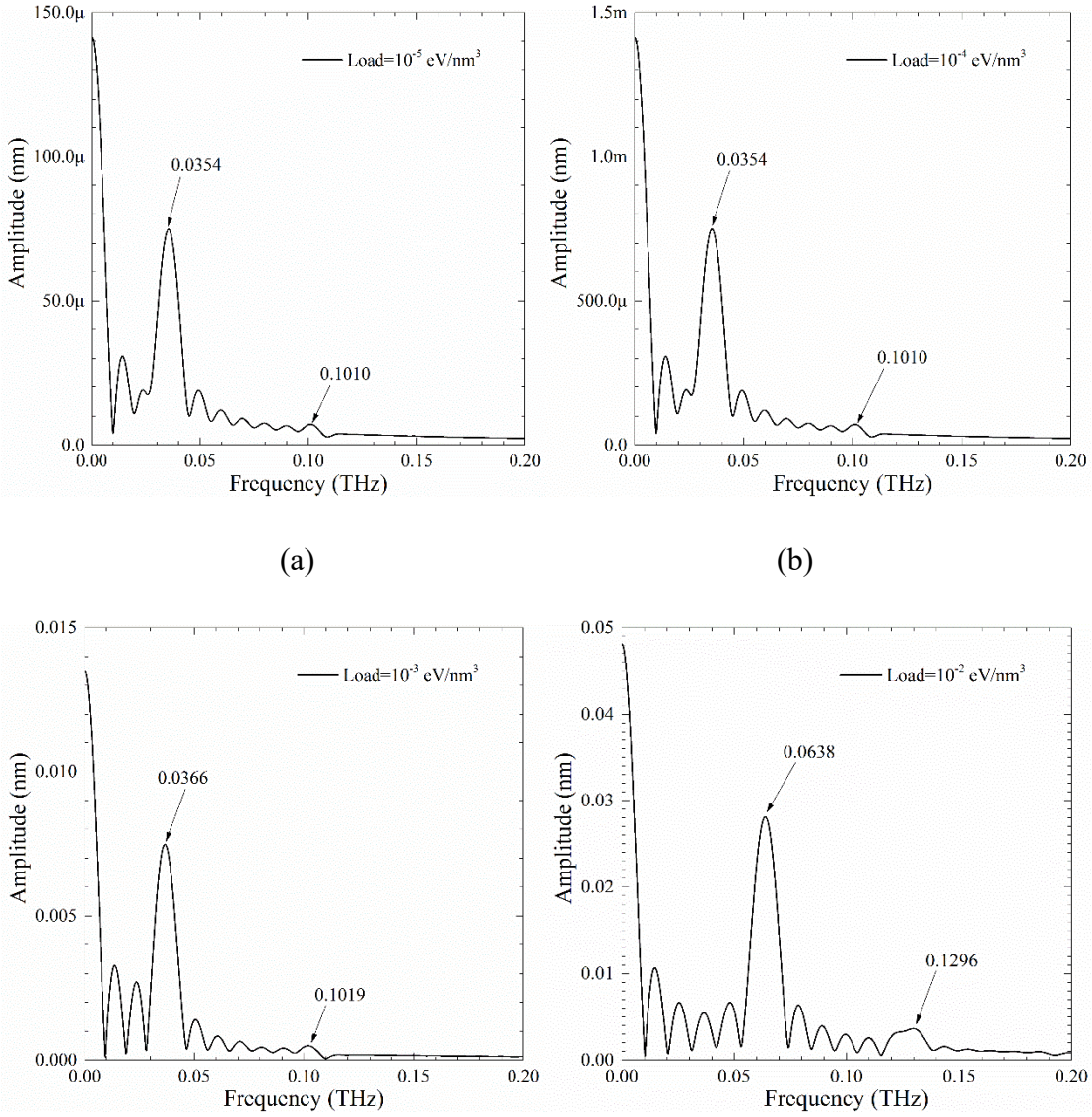

Fig. 5. Frequency spectra for a (20, 20)/(20, 0) simply-supported graphene sheet under various external loads.

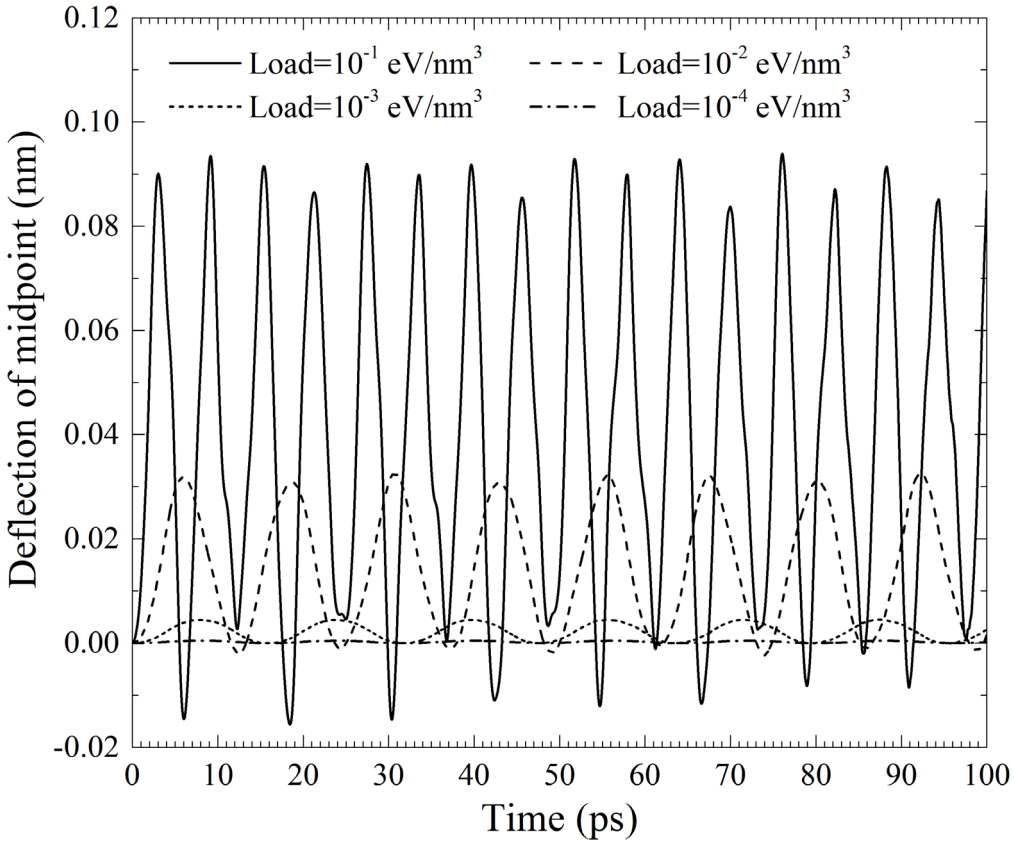

Fig. 6. Time history responses of a (15, 15)/(15, 0) simply-supported graphene sheet under various external loads. The time step is set as 5 *f*s.

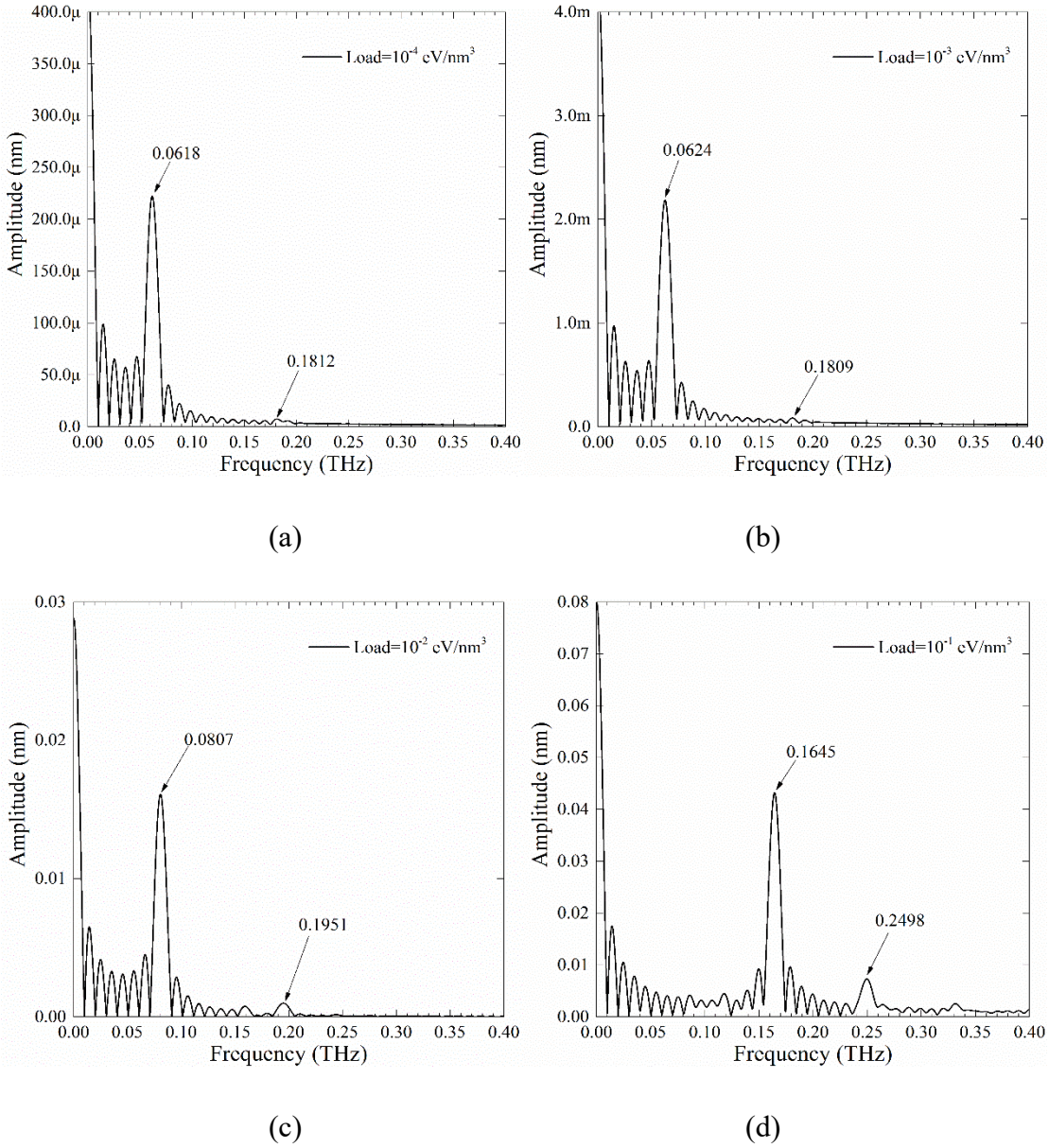

Fig. 7. Frequency spectra for a (15, 15)/(15, 0) simply-supported graphene sheet under various external loads.

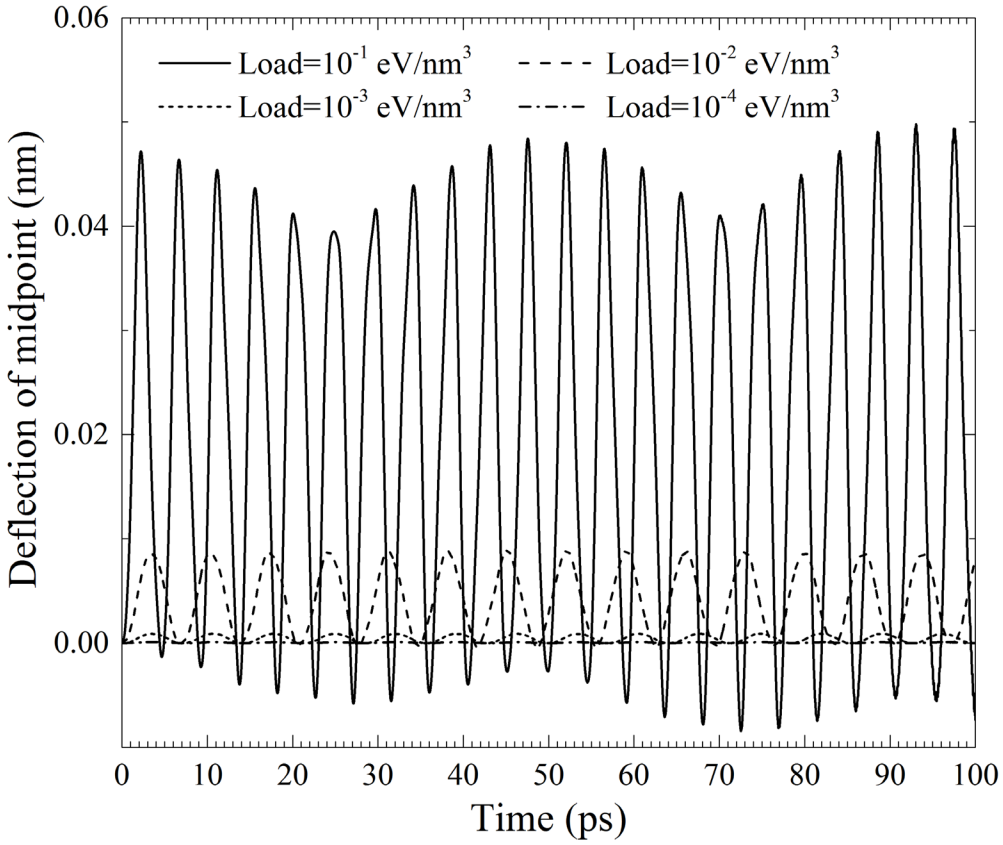

Fig. 8. Time history responses of a (10, 10)/(10, 0) simply-supported graphene sheet under various external loads. The time step is set as 5 *f*s.

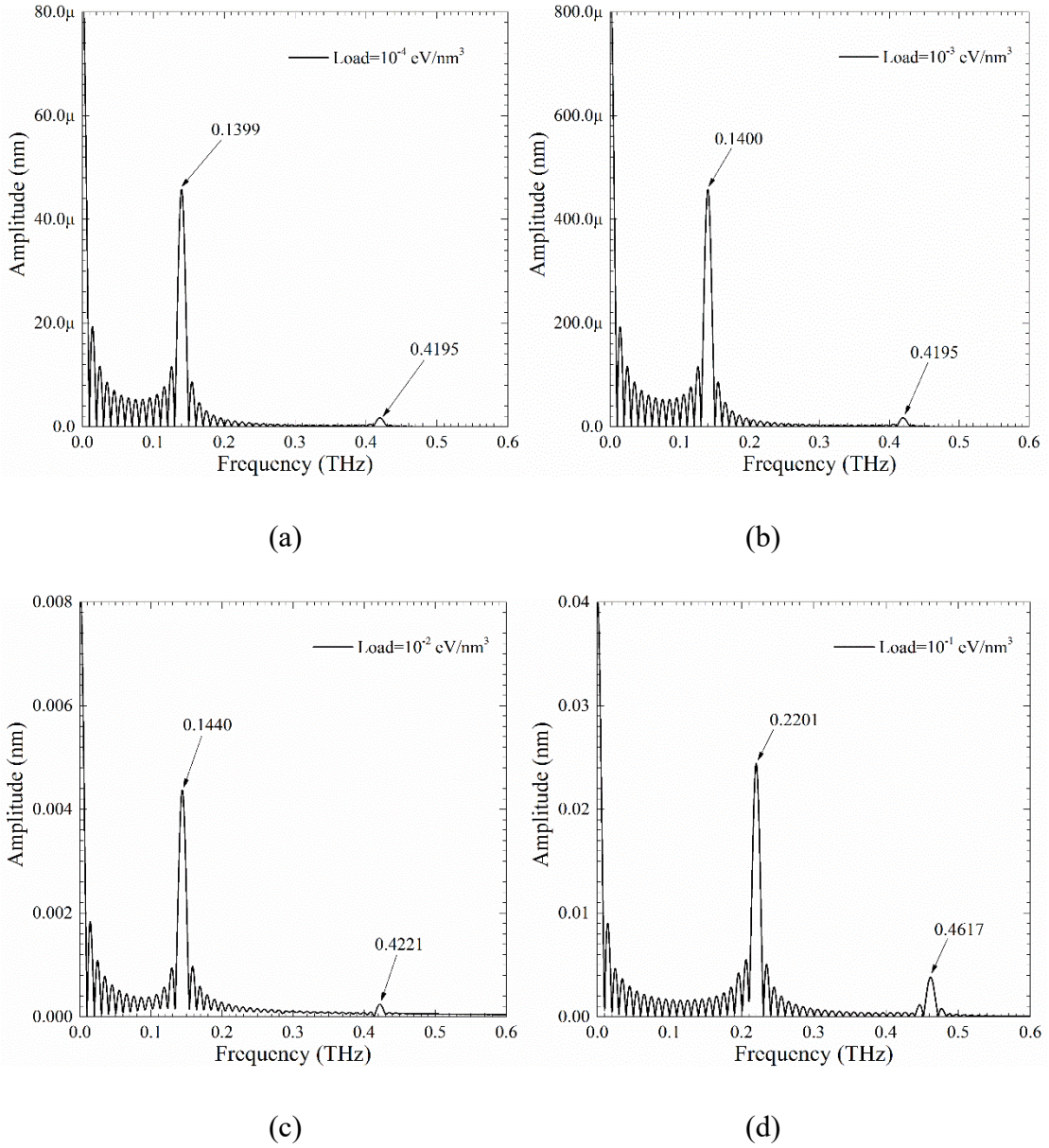

Fig. 9. Frequency spectra for a (10, 10)/(10, 0) simply-supported graphene sheet under various external loads.

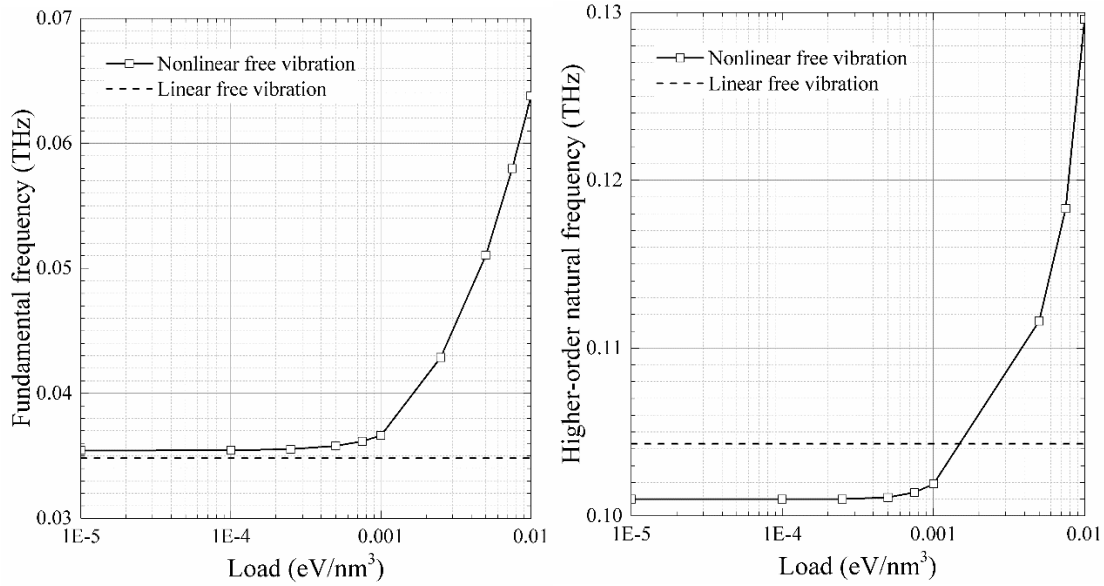

Fig. 10. Linear and nonlinear fundamental frequencies of a (20, 20)/(20, 0) simply-supported graphene sheet under various external loads.

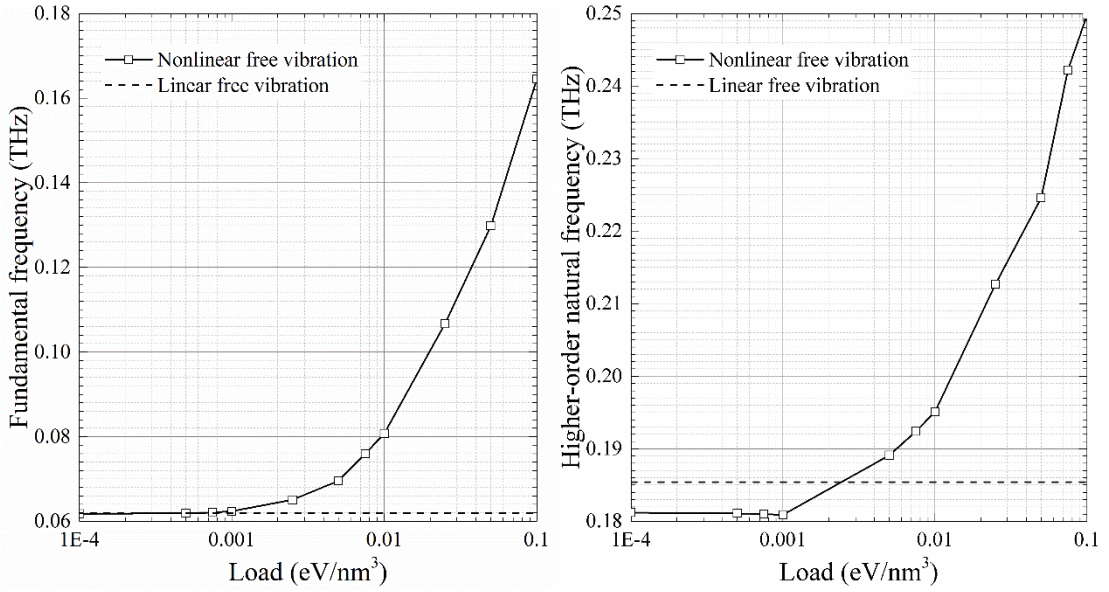

Fig. 11. Linear and nonlinear fundamental frequencies of a (15, 15)/(15, 0) simply-supported graphene sheet under various external loads.

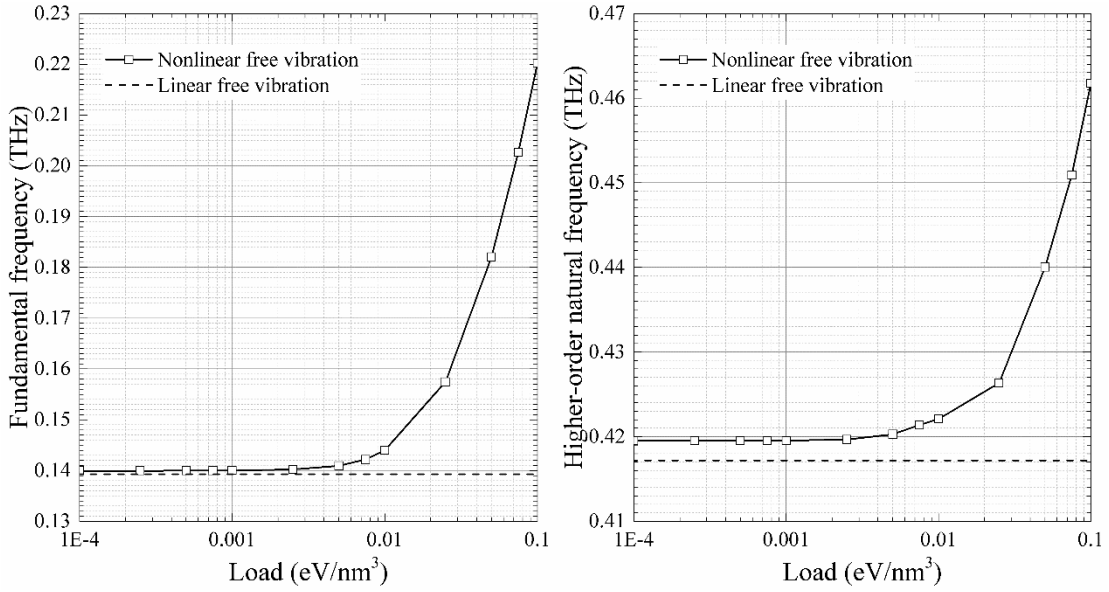

Fig. 12. Linear and nonlinear fundamental frequencies of a (10, 10)/(10, 0) simply-supported graphene sheet under various external loads.

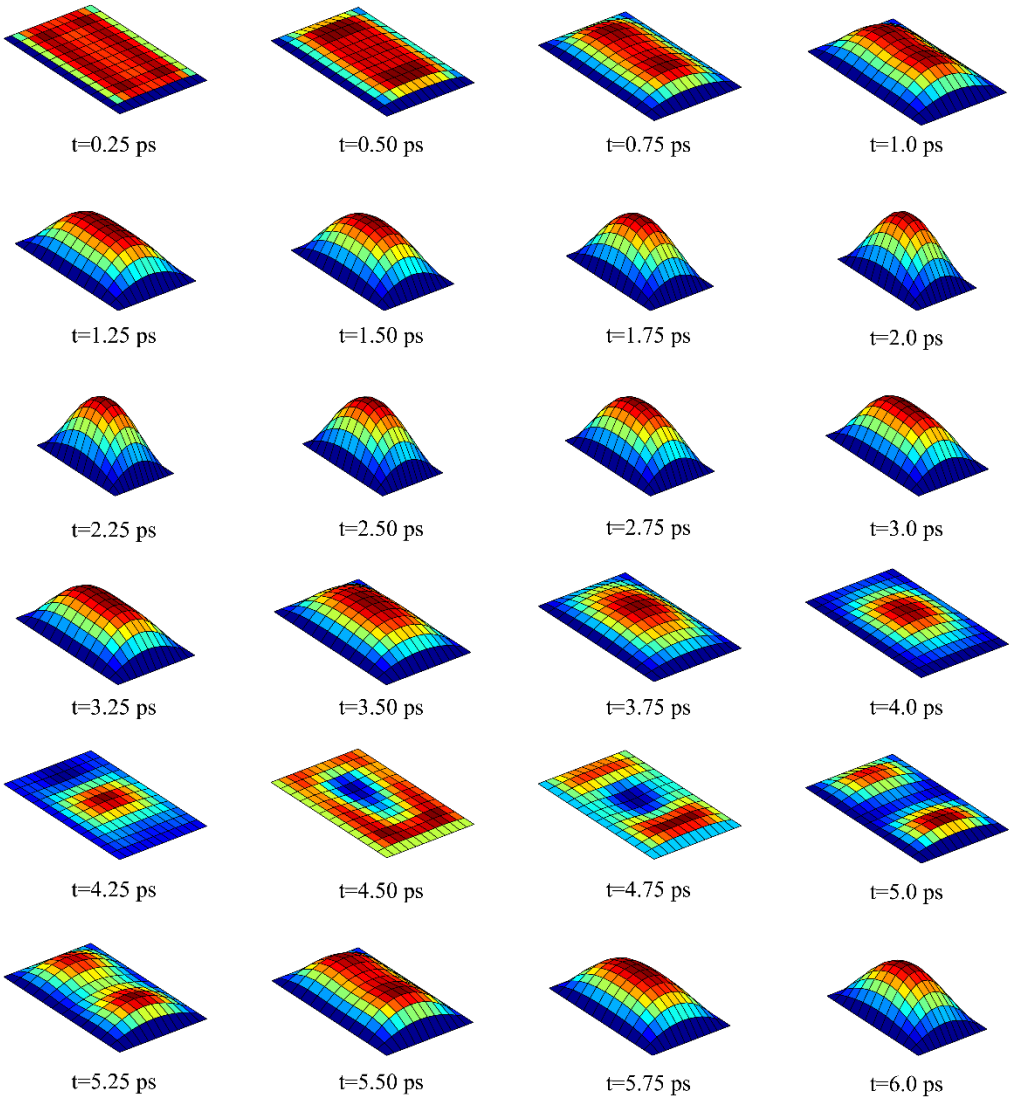

Fig. 13. Surface morphology evolution of a (10, 10)/(10, 0) simply-supported graphene sheet under a uniformly distributed load of 0.1 eV/nm^3.

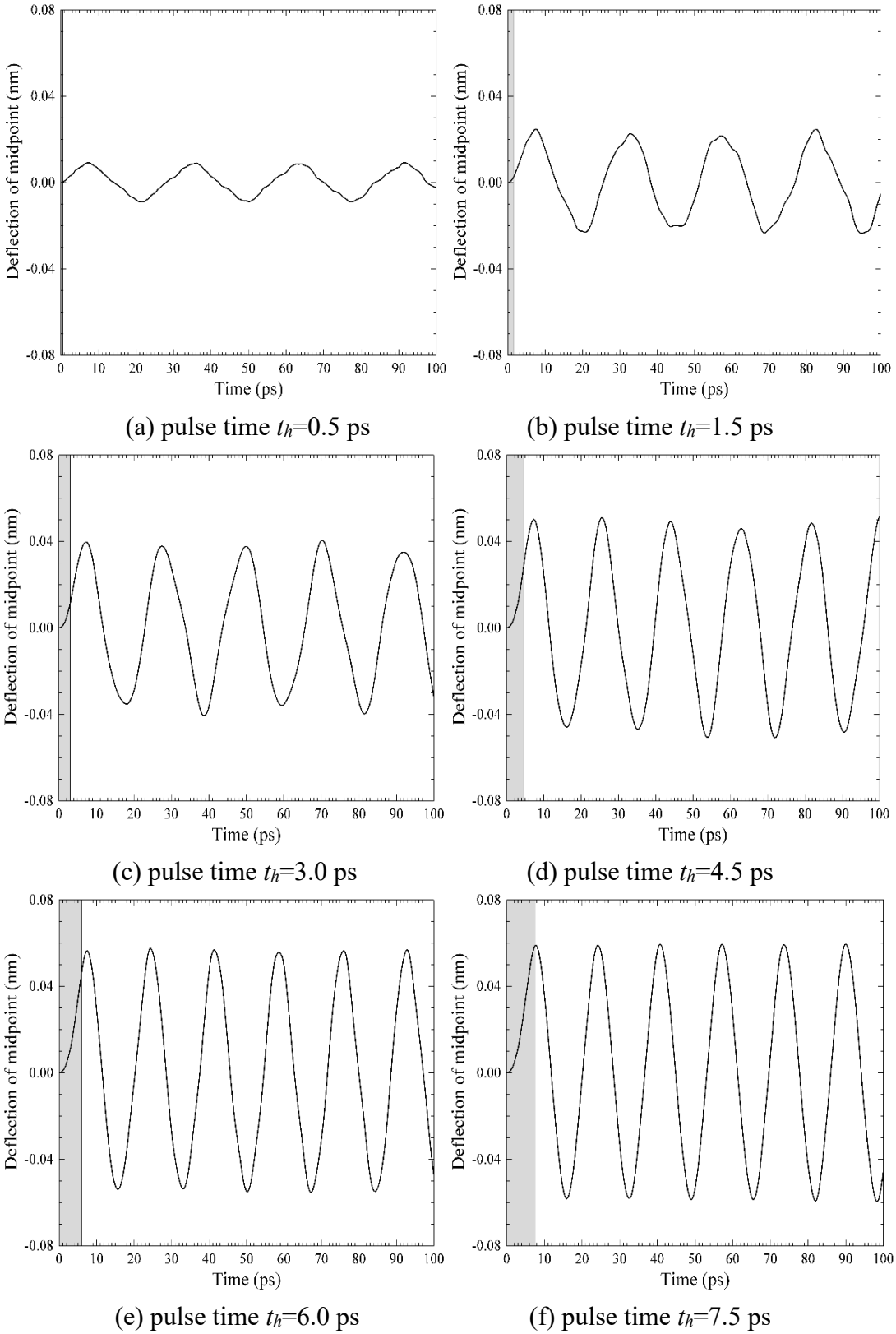

(a) pulse time t_h=0.5 ps (b) pulse time t_h=1.5 ps

(c) pulse time t_h=3.0 ps (d) pulse time t_h=4.5 ps

(e) pulse time t_h=6.0 ps (f) pulse time t_h=7.5 ps

Fig. 14. Time history responses of a (20, 20)/(20, 0) simply-supported graphene sheet under 0.01 eV/nm^3 at different pulse time t_h.

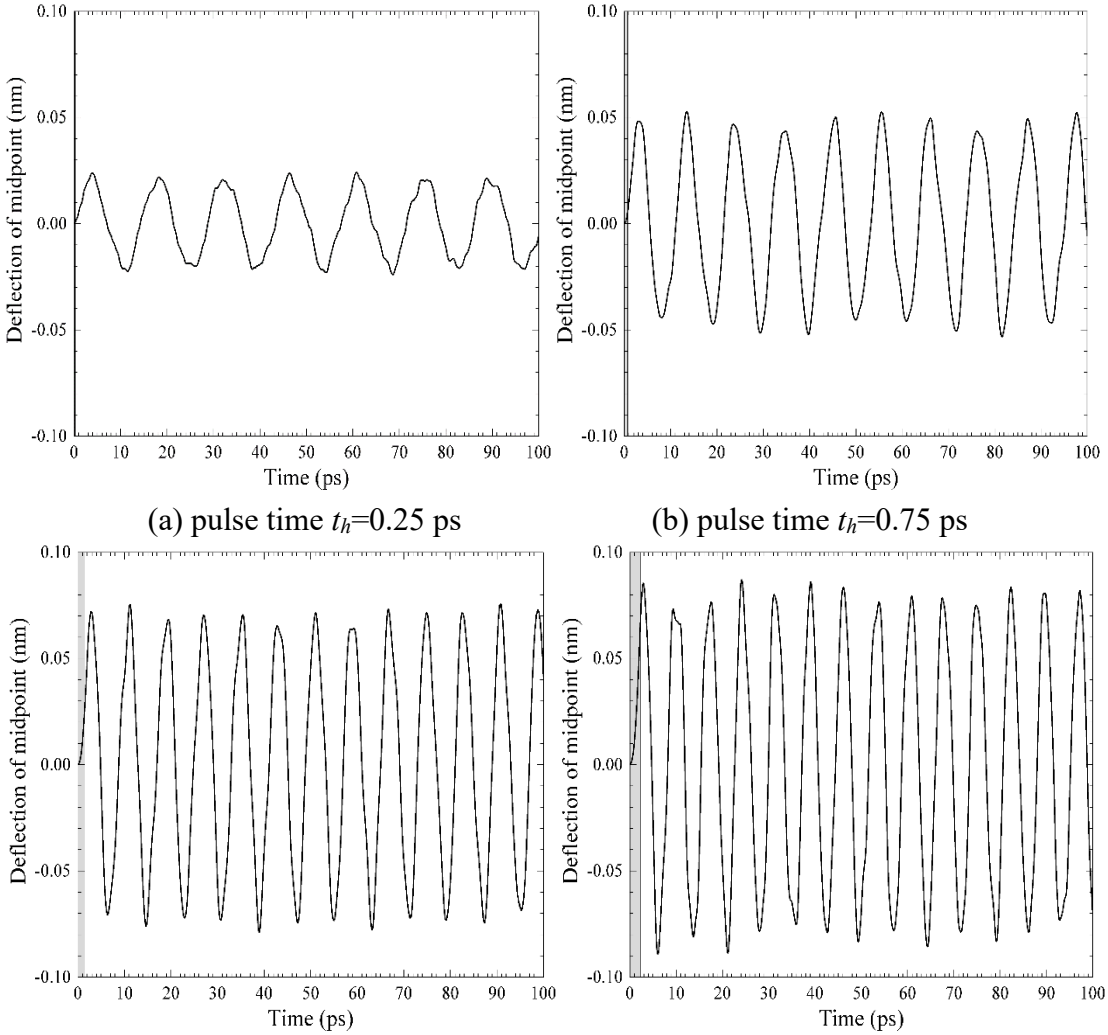

(a) pulse time t_h=0.25 ps (b) pulse time t_h=0.75 ps

(c) pulse time t_h=1.5 ps (d) pulse time t_h=2.25 ps

Fig. 15. Time history responses of a (15, 15)/(15, 0) simply-supported graphene sheet under 0.1 eV/nm^3 at different pulse time t_h.

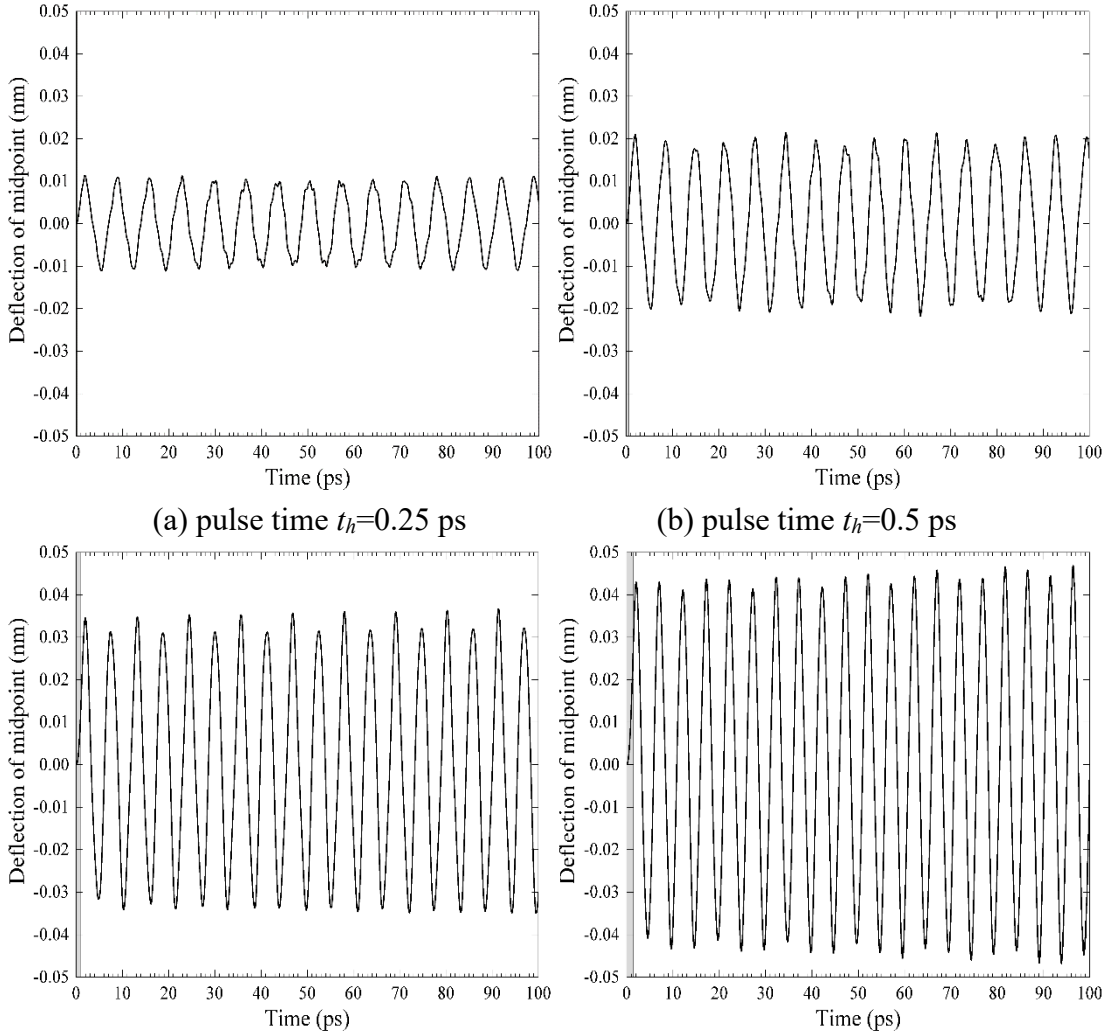

(a) pulse time t_h=0.25 ps (b) pulse time t_h=0.5 ps

(c) pulse time t_h=1.0 ps (d) pulse time t_h=1.5 ps

Fig. 16. Time history responses of a (10, 10)/(10, 0) simply-supported graphene sheet under 0.1 eV/nm^3 at different pulse time t_h.

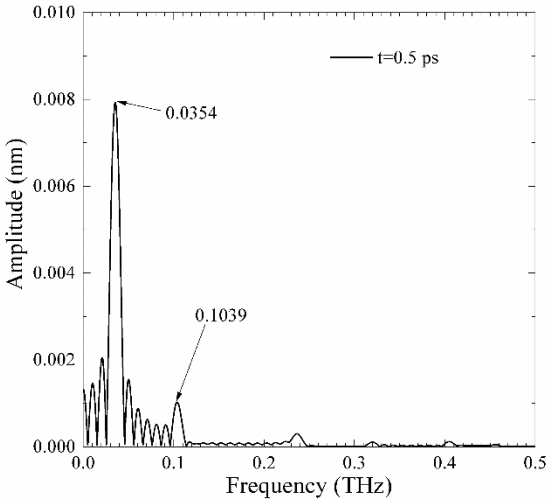
t=0.5 ps
0.0354
0.1039
Amplitude (nm)
Frequency (THz)

(a)

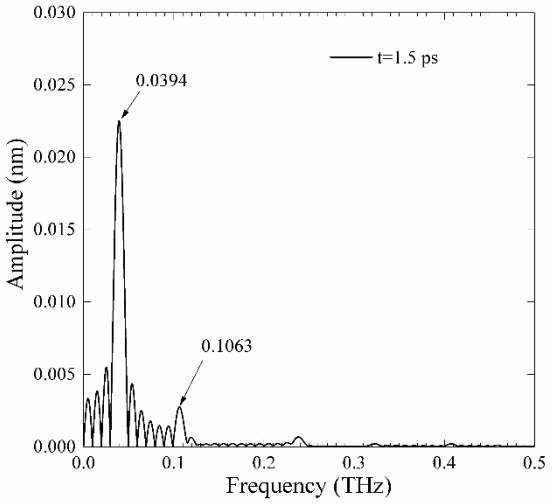
t=1.5 ps
0.0394
0.1063
Amplitude (nm)
Frequency (THz)

(b)

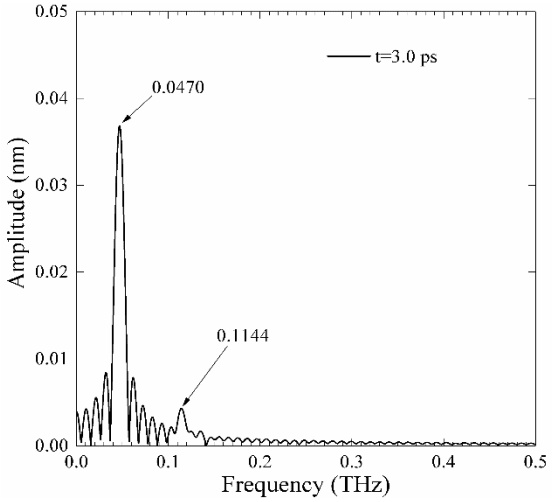
t=3.0 ps
0.0470
0.1144
Amplitude (nm)
Frequency (THz)

(c)

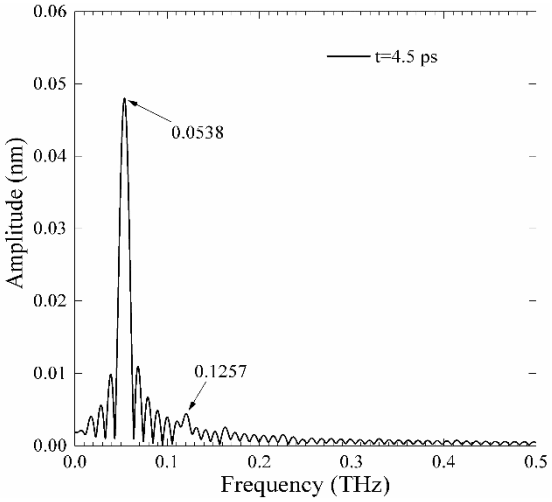
t=4.5 ps
0.0538
0.1257
Amplitude (nm)
Frequency (THz)

(d)

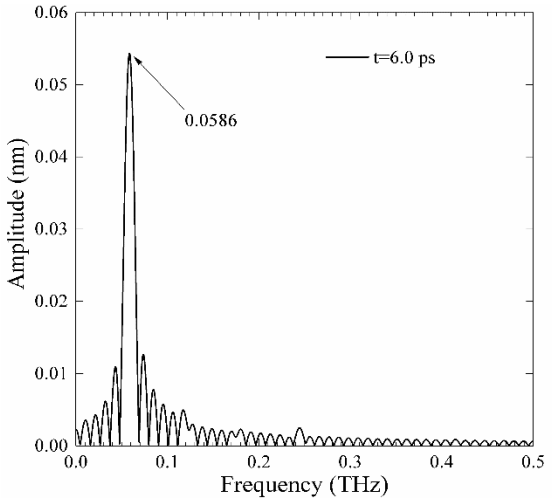
t=6.0 ps
0.0586
Amplitude (nm)
Frequency (THz)

(e)

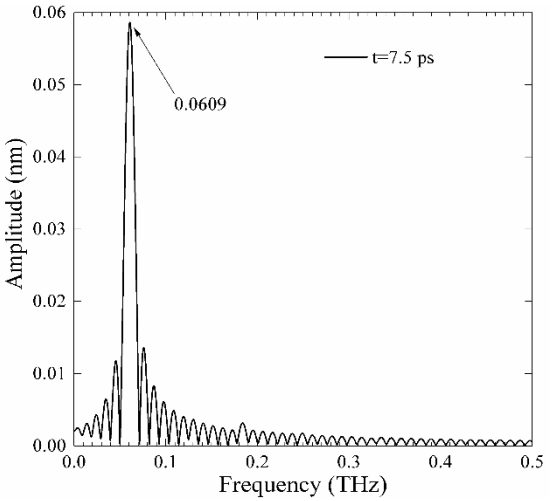
t=7.5 ps
0.0609
Amplitude (nm)
Frequency (THz)

(f)

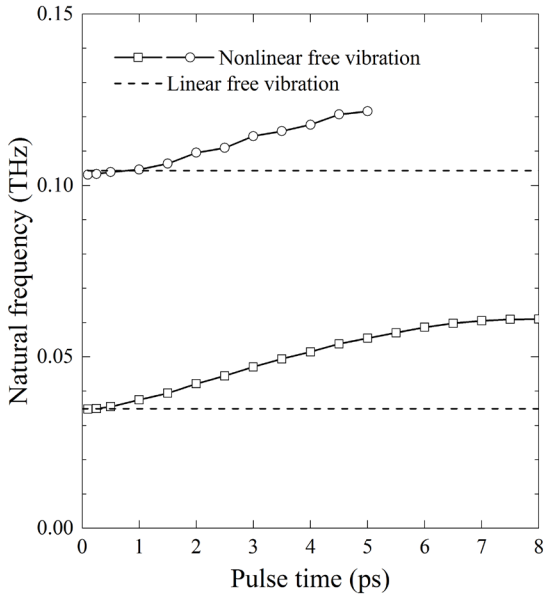

(g)

Fig. 17. Frequency spectra for a (20, 20)/(20, 0) simply-supported graphene sheet under 0.01 eV/nm^3 at different pulse time (a)-(f), and natural frequency versus pulse time (g).

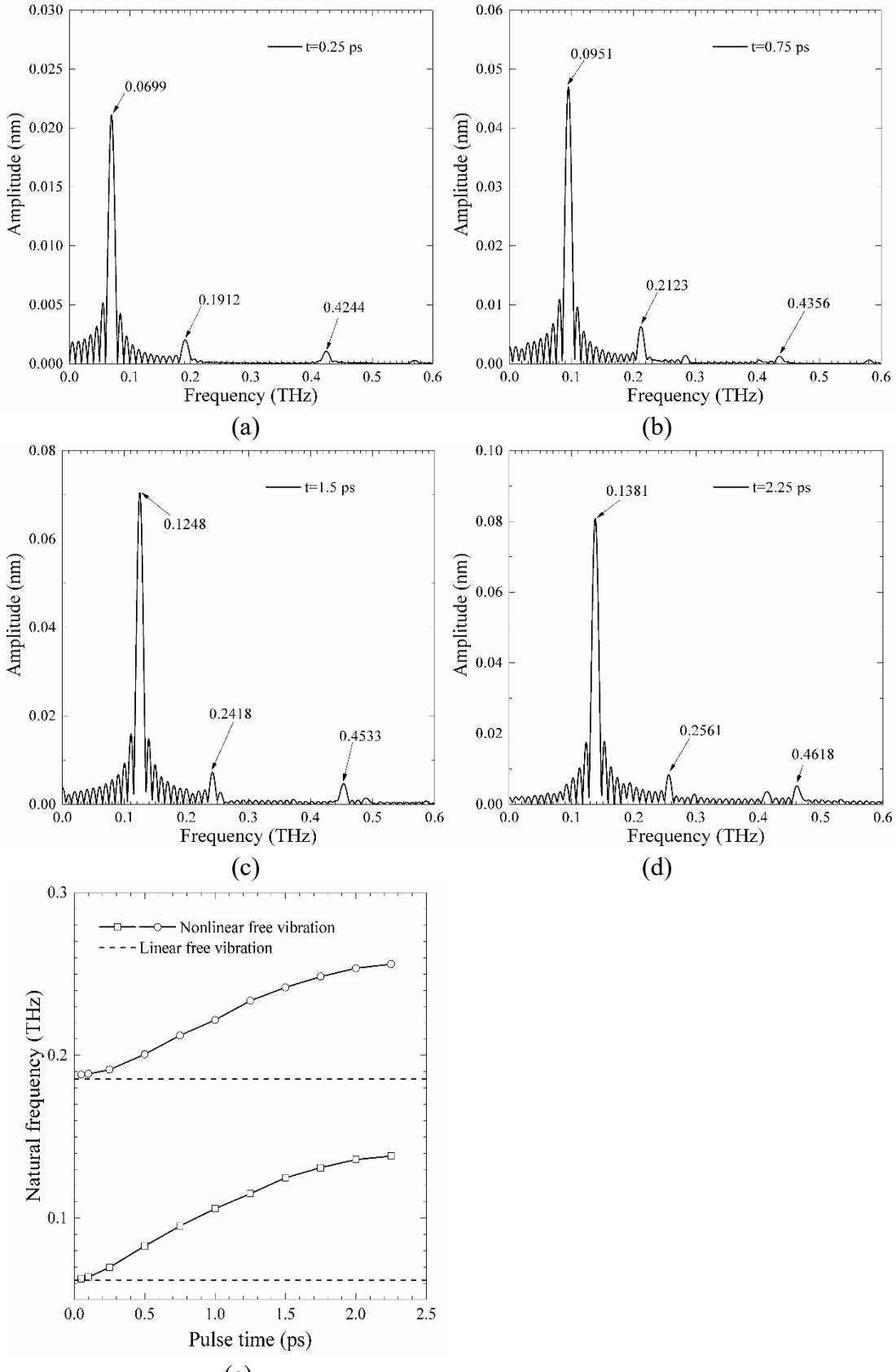

Fig. 18. Frequency spectra for a (15, 15)/(15, 0) simply-supported graphene sheet under 0.1 eV/nm^3 at different pulse time (a)-(d), and natural frequency versus pulse time (e).

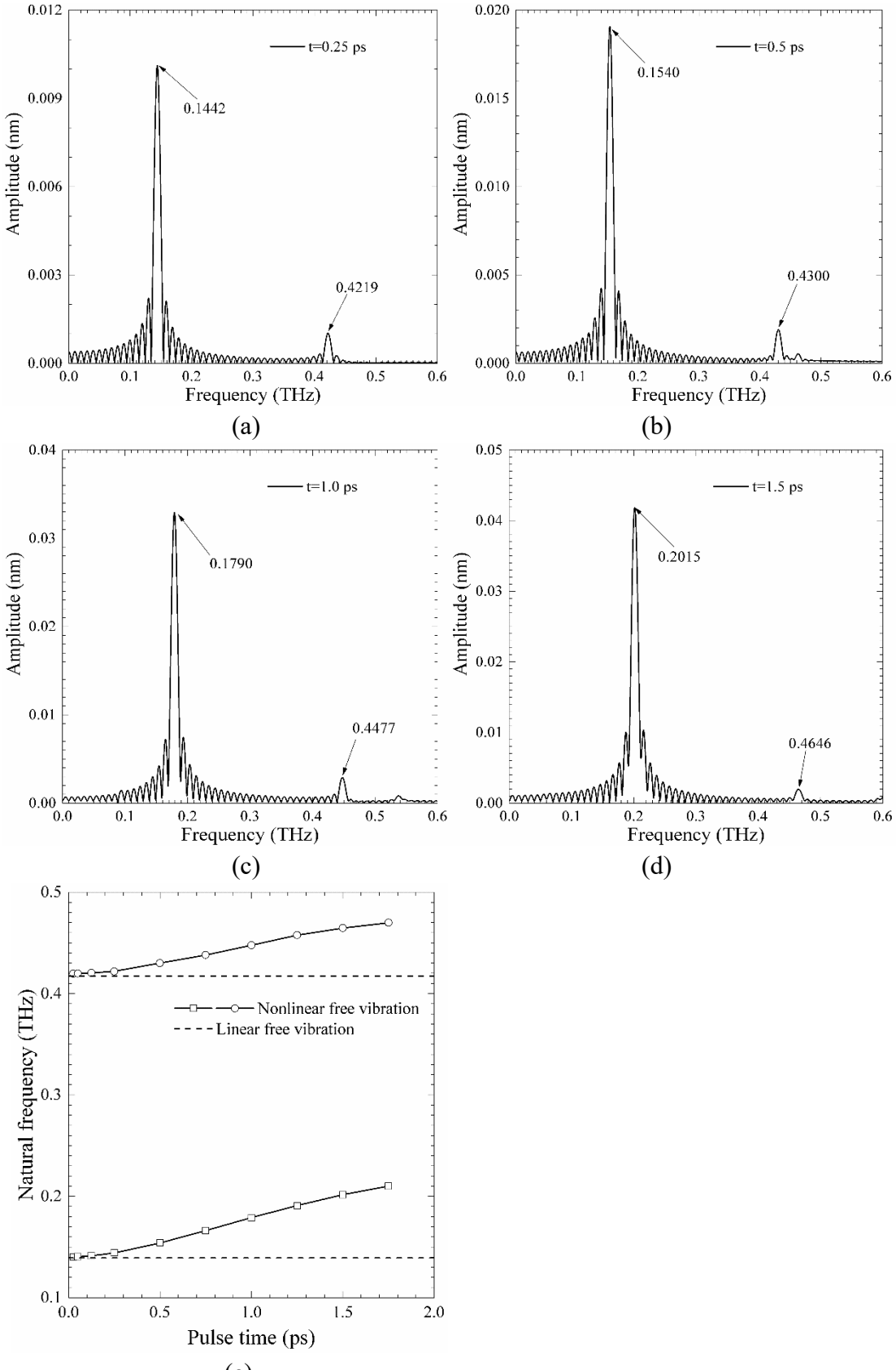

Fig. 19. Frequency spectra for a (10, 10)/(10, 0) simply-supported graphene sheet under 0.1 eV/nm^3 at different pulse time (a)-(d), and natural frequency versus pulse time (e).